

MATHEMATICAL MODELLING OF THE ONSET OF TRANSFORMATION
FROM AUSTENITE TO PEARLITE UNDER NON-CONTINUOUS COOLING
CONDITIONS

by

TRI TUC PHAM

B.Sc., Monash University, Australia 1985

B.E., Monash University, Australia 1987

A THESIS SUBMITTED IN PARTIAL FULFILLMENT OF

THE REQUIREMENTS FOR THE DEGREE OF

MASTER OF APPLIED SCIENCE

in

THE FACULTY OF GRADUATE STUDIES

(Department of Metals and Materials Engineering)

We accept this thesis as conforming

to the required standard

THE UNIVERSITY OF BRITISH COLUMBIA

April, 1993

© T. T. Pham, 1993

In presenting this thesis in partial fulfilment of the requirements for an advanced degree at the University of British Columbia, I agree that the Library shall make it freely available for reference and study. I further agree that permission for extensive copying of this thesis for scholarly purposes may be granted by the head of my department or by his or her representatives. It is understood that copying or publication of this thesis for financial gain shall not be allowed without my written permission.

(Signature)

Department of METALS & MATERIALS

The University of British Columbia
Vancouver, Canada

Date April 15, 1993

ABSTRACT

The temperature at which a new phase forms is an important parameter in the genesis of final microstructure. For diffusional transformation processes, prediction of this temperature on cooling, until now, relied upon empirical equations which are based on the cooling rate or degree of undercooling.

To develop a method that is capable of predicting the onset of transformation in the steel, applicable to industrial processing conditions, a theoretical study has been conducted to critically examine the consequences and implications of the Scheil additivity rule in relation to the incubation of the austenite decomposition. An "ideal" isothermal transformation curve for the start of transformation from austenite to pearlite has been developed based on the assumption of the consumed fractional incubation time being additive. The curve is characteristic of the chemistry and the austenite grain size of the steel. A mathematical relationship between the experimental time to the start of transformation and the ideal incubation time was quantified, and two methods for deriving an "ideal" *TTT* curve from the controlled cooling experiments were established in this study.

The derived "ideal" *TTT* curve was used for predicting the start of transformation from austenite to pearlite for three different cooling conditions; namely, continuous, semi-continuous and non-continuous cooling conditions. The predictions were consistent in all cases and compared favourably against other methods which have been employed frequently to estimate the transformation start temperature for non-isothermal conditions.

Table of Contents

ABSTRACT	ii
Table of Contents	iii
Table of Tables	v
Table of Figures	vi
NOMENCLATURE	ix
ACKNOWLEDGEMENTS	xii
Chapter 1 INTRODUCTION	1
Chapter 2 REVIEW OF THE LITERATURE	4
2.1 The Onset of the Austenite Decomposition	4
2.2 Inter-Relation of Cooling & Isothermal Transformation Behaviour	6
2.3 Criteria for the Additivity	11
2.4 The Incubation Time	14
2.4.1 Classical Nucleation Theory	15
2.4.2 The Growth Equation	20
2.5 Contemporary Approaches	24
Chapter 3 OBJECTIVES AND SCOPE OF THE STUDY	30
Chapter 4 INCUBATION TIME AND THE ADDITIVITY PRINCIPLE	33
4.1 The "Ideal" <i>TTT</i> Curve for the Incubation	34
4.1.1 Measurement of The "Ideal" Incubation Time	40
4.2 Calculation of The "Ideal" Incubation Time from Cooling Data	42

Chapter 5	EXPERIMENTAL DESIGN	45
5.1	Materials	45
5.2	Isothermal and Cooling Apparatus	48
5.3	Isothermal and Cooling Test Procedures	51
5.3.1	Cooling Schedules	51
5.3.2	Analysis of Experimental Data	56
Chapter 6	RESULTS AND DISCUSSIONS	57
6.1	Initial and Final Microstructures	57
6.2	The "Ideal" Incubation Time	61
6.2.1	Application of Inverse Additivity	61
6.2.2	Expression of The Ideal Incubation Time	64
6.3	Predicting The Start of Transformation to Pearlite	72
6.3.1	Based on The "Ideal" Incubation Time	72
6.3.2	By Conventional Methods	78
6.3.2.1	Using Cooling Rates at Ae_1	78
6.3.2.2	Based on Experimental TTT Results	81
6.3.3	Prediction Capability of the Three Methods	85
Chapter 7	SUMMARY AND RECOMMENDATION	87
7.1	Summary of The Study	87
7.2	Recommendation for Further Development	89
REFERENCES	91
APPENDICES	99
A.1	Thermal Analysis of the Tubular Specimen	99

A.2 Thermal Gradient inside the Tubular Specimen	104
A.3 Determination of the Transformation Start	105

Table of Tables

Table 5.1:	Composition of steel used in this study.	45
Table 6.1:	Experimental times obtained from the controlled isothermal experiments.	70

Table of Figures

Figure 2.1:	An early representation of the relationship between the cooling rate and the transformation start temperature by Bain ^[36]	5
Figure 2.2:	Schematic illustration of the Grange-Keifer method of predicting the transformation start under continuous cooling conditions	10
Figure 2.3:	Free energy of cluster (pre-nucleation) formation	16
Figure 2.4:	Schematic composition profile across the pearlite lamella and austenite interface	21
Figure 4.1:	Schematic illustration of the relationship between the "ideal" and experimental incubation time at temperature T_i	35
Figure 4.2:	Interrelationship between the continuous cooling, experimental and "ideal" isothermal starting time	39
Figure 4.3:	Schematic illustration of the relationship between the "ideal" and experimental incubation time	41
Figure 5.1:	The modified $Fe(X)-C$ phase diagram for the eutectoid steel having the composition shown in Table 5.1	46
Figure 5.2:	Microstructure of the eutectoid steel after being heat treated to minimise the compositional variation. Mag. x800	47
Figure 5.3:	The testing chamber of the Gleeble 1500: a) Overview of the test chamber, b) Enlargement showing dilatometer specimen, specimen holder and LVDT C-Strain device assembly	50
Figure 5.4:	Schematic diagram showing cooling schedules for: i) controlled cooling, ii) conventional isothermal, iii) controlled isothermal and, iv) stepped isothermal tests.	55

Figure 6.1:	Microstructure of the austenitised, quenched specimen etched in alkaline sodium picrate to reveal the prior austenite grain boundaries. (a) optical micrograph at a magnification x1000, (b) outline of the grain boundaries.	58
Figure 6.2:	SEM microstructure of a specimen control cooled at 3 °C/s to 680 °C, isothermally transformed to pearlite and air cooled to room temperature. Magnification x2000.	59
Figure 6.3:	SEM microstructure of a specimen rapidly cooled to 650 °C, isothermally transformed to pearlite and air cooled to room temperature. Magnification x3000.	59
Figure 6.4:	SEM microstructure of a specimen air cooled to room temperature by natural convection and radiation, showing primarily pearlite structure. Magnification x4000.	60
Figure 6.5:	Continuous cooling transformation diagram for eutectoid steel under constant cooling rate conditions.	61
Figure 6.6:	Constant cooling rate to reach a given undercooling prior to transformation.	63
Figure 6.7:	The "ideal" incubation time as a function of undercooling.	63
Figure 6.8:	Logarithmic plot of the product of incubation time and $\exp(-Q/RT)$ as a function of undercooling below A_{e_f}	65
Figure 6.9:	The "ideal" isothermal transformation (<i>TTT</i>) diagram.	66
Figure 6.10:	Comparison of the derived ideal <i>TTT</i> curve to the curve for 0.1% transformation by Kirkaldy & Venugopalan. ^[79]	69
Figure 6.11:	Comparison of the derived ideal <i>TTT</i> curve with the published literature for a 1080 <i>TTT</i> curve. ^[29]	69
Figure 6.12:	Thermal histories of the Newtonian cooling situations used in this study.	74
Figure 6.13:	Simulation of rod cooling on a Stelmor conveyor.	74
Figure 6.14:	Predicted and measured transformation start under Newtonian coolings and Stelmor simulation conditions.	75

Figure 6.15:	Predicted and measured transformation start for non-continuous cooling conditions.	77
Figure 6.16:	Correlation between the transformation start temperature and the cooling rate.	79
Figure 6.17:	Predicted and measured transformation start times under the Newtonian coolings and Stelmor simulation conditions, using cooling rates at the Ae_I	79
Figure 6.18:	The experimental <i>TTT</i> curves.	82
Figure 6.19:	Predicted and measured transformation start times for the two Newtonian coolings and the Stelmor condition, based on the experimental <i>TTT</i> curve.	84
Figure 6.20:	Predicted and measured transformation start times under the non-continuous cooling conditions, based on experimental <i>TTT</i> curves.	84
Figure A.1-1:	Thermal history of a specimen that was rapidly cooled to 650 °C where it is held isothermally	A-5
Figure A.2-1:	Thermal and dilation history of a specimen undergoing controlled cooling at 3 °C/s, after being isothermally held at 780 °C for 1 minute	A-7
Figure A.2-2:	Relationship between the dilation and temperature throughout the experiment, with a linear correlation exists in the pre-transformed region	A-8
Figure A.2-3:	Deviation of the measured data from the linear regression, delineating the start of transformation to pearlite	A-9

NOMENCLATURE

<i>Symbol</i>	<i>Description</i>	<i>Unit</i>
A_{Cm}	Equilibrium temperature between the austenite (γ) and cementite (Fe_3C), or the γ/Fe_3C phase boundary.	$^{\circ}C$
Ae_1	Equilibrium temperature between the austenite (γ) and pearlite.	$^{\circ}C$
Ae_3	Equilibrium temperature between the austenite (γ) and ferrite (α), or the γ/α phase boundary.	$^{\circ}C$
$C^*_{\alpha\gamma}$	Interfacial composition of carbon just ahead of the ferrite lammellar.	<i>at. % of C</i>
$C^*_{Fe_3C\gamma}$	Interfacial composition of carbon just ahead of the cementite lammellar.	<i>at. % of C</i>
C_{Fe_3C}	Carbon concentration in the cementite lammellar.	<i>at. % of C</i>
ΔC	Lateral carbon concentration difference just ahead of the pearlite lammella.	<i>at. % of C</i>
D	Diffusion coefficient, or diffusivity.	m^2/sec
D_{eff}	Effective diffusivity.	m^2/sec
D_{γ}	Prior austenite grain size.	μm
$F(T, \chi)$	Arbitrary rate reaction function which is dependent on temperature and volume fraction transformed.	
$G(T)$	Arbitrary function which depends only on temperature.	
$\Delta G(n), \Delta G_v$	Gibbs free energy change associated with nucleus formation.	J/m^3
\dot{G}	Growth rate.	$sec.^{-1}$
$H(\chi)$	Arbitrary function which depends only on the volume fraction transformed.	

NOMENCLATURE

k	Boltmann's constant.	$J/atom. ^\circ K$
l	Effective diffusion distance.	m
$\dot{N}_{cm}, \dot{N}_{edg}$	Nucleation rate density at grain corners, along grain edges and grain surfaces, respectively.	m^{-3}
$\&\dot{N}_{sfc}$		
$\dot{N}(t)$	Time dependence nucleation rate density.	m^{-3}
N_0	Number of available nucleation sites.	
\dot{N}_s	Steady state nucleation rate density.	m^{-3}
Q	Activation enthalpy for diffusion.	J/mol
Q_{eff}	Effective activation enthalpy for diffusion.	J/mol
R	Gas constant.	$J/mol. ^\circ K$
t	Transformation time.	$sec.$
t_0	Cooling time to the equilibrium temperature.	$sec.$
$t_{0.5}$	Time for completion of one half of the transformation.	$sec.$
t_c	Cooling time to the reach the test temperature.	$sec.$
t_{CCT}	Total cooling time from the equilibrium temperature to the onset of transformation.	$sec.$
t_{eq}	Equivalent time.	$sec.$
t_{IT}	Isothermal holding time to the onset of transformation.	$sec.$
t_r	The time required for a nucleus to form/decompose, based on "time reversal" principle.	$sec.$
t_s	Total time to the start of the transformation.	$sec.$
T	Temperature.	$^\circ C$
T^*	Mean temperature between T_{IT} and T_{CCT} .	$^\circ C$
T_0	Equilibrium temperature.	$^\circ C$

NOMENCLATURE

T_{CCT}	Temperature at which a continuous cooling path intersects the continuous cooling transformation curve.	$^{\circ}C$
T_{IT}	Temperature at which a continuous cooling path intersects the isothermal transformation curve.	$^{\circ}C$
T_s	Solution treating temperature.	$^{\circ}C$
T_t	Isothermal test temperature	$^{\circ}C$
ΔT	Degree of undercooling, or the amount of the difference in temperature below the equilibrium.	$^{\circ}C$
ΔT_{CCT}	Magnitude of the undercooling at which the new phase forms on cooling.	$^{\circ}C$
ν_p	The rate of pearlite growth.	sec^{-1}
ν_s	Rate for establishing the steady state nucleation condition.	sec^{-1}
Z	Zeldovich non-equilibrium factor ($\cong 10^{-2}$)	
β	Rate at which atoms are attached to the critical nucleus.	sec^{-1}
τ	Incubation time.	$sec.$
$\tau(T)$	Incubation time as a function of temperature.	$sec.$
τ_G	Isothermal growth time of pearlite.	$sec.$
τ_i	Incubation time at the i^{th} iteration.	$sec.$
τ_s	Induction period necessary for establishing steady state nucleation.	$sec.$
τ_t	Incubation time at the test temperature.	$sec.$
$\dot{\theta}$	Cooling rate.	$^{\circ}C/sec.$
$\dot{\theta}_i$	Cooling rate i .	$^{\circ}C/sec.$
$\dot{\theta}_{Ci}$	Constant cooling rate i .	$^{\circ}C/sec.$
χ	Volume fraction transformed of the new phase.	

ACKNOWLEDGEMENTS

This study has been conducted with financial assistance from BHP Research and Rod and Bar Product Division, Australia. I would like to particularly thank the Product Development Group and Rod Mill Personnel of RBPD, and the Melbourne Laboratories for the support that has enabled us to gain another step in understanding the transformation in steel.

This collaborative project was initiated by the enthusiastic effort of Professor Bruce Hawbolt during his sabbatical leave to the Melbourne Laboratories of BHP Research in early 1990. I sincerely thank him for his continued effort in making this project realised.

The friendship and help offered by my fellow students and colleagues have made my time at UBC rewarding, and our stay in Vancouver memorable. There are many of you, the list is endless, each in your own way have accepted and made us feel welcomed during the last two years.

The caring support and thoughtfulness of my wife, Kathleen, has been a constant source of comfort and encouragement, especially, during the course of this study. And thanks to my daughter, Isabel, who was born during the writing of this thesis, has given me the added incentive to complete it. May tomorrow always bring her happiness.

Chapter 1

INTRODUCTION

In the early 1960's, the application of accelerated cooling as part of a thermochemical processing strategy resulted in a significant improvement in the final properties of steel products.^[1,2] The enhancement of the mechanical properties of accelerated cooled products has been attributed to two major metallurgical factors: significant refinement of ferrite grain size, and the formation of lower temperature acircular ferrite, fine pearlite or bainitic transformation products.^[3-5]

The improvement of mechanical properties through microstructure refinement enables steel products of the same strength to be produced with lower alloying addition. This not only reduces the cost of producing steels, but also allows steels of lower carbon equivalent levels to be used, resulting in an improvement in weldability. The potential metallurgical benefits which could be attained through accelerated cooling have become apparent to the international metallurgical community in recent years, and have spawned a considerable amount of research and development in various aspects of this technology.^[6-11]

Recent advances in thermomechanical treatment and controlled rolling further emphasize the role of accelerated cooling in optimising the final properties of the product. A considerable effort has been devoted to incorporating the accelerated cooling strategy to the thermomechanical processing routes, in order to further refine the final microstructure, and hence, produce improved properties.^[12-18]

Through the application of such innovative processing schedules, the achievement of ultrafine equiaxed ferrite grain size ($< 5 \mu\text{m}$) under laboratory conditions has been reported.^[17,18] The particular mechanism which is responsible for yielding the ultrafine microstructure is yet to be fully understood theoretically. However, it is qualitatively correct that the final microstructure of a steel product depends primarily on the state of the austenite prior to transformation and the temperature at which the austenite decomposes.

The state of the austenite is defined by a number of variables, including the history of the deformation imposed upon the steel and the morphology of the austenite grain; each have an influence in modifying the rate at which the new phase forms.^[16,19-23]

The temperature at which the transformation begins is the most critical parameter. It dictates the amount of driving force available for nucleation and governs the rate of growth and coarsening of the new phase, hence, the scale of the final microstructure.^[5,20-22] This temperature is invariably lowered when the cooling rate from the hot rolling temperature is increased. However, as yet there is no theoretical determination for the transformation start temperature obtained under non-isothermal conditions, although various expressions have been empirically derived based on steel chemistry and cooling rate,^[15] degree of undercooling^[24] or product thickness.^[13]

For accelerated or controlled cooling situations in which the cooling rate does not remain continuous during the cooling process, e.g. Stelmor,^[1,24] Tempcore^[25,26] and other interrupted cooling processes,^[27] determination of the transformation start temperature has become increasingly difficult even using empirical methods.

To better understand the microstructural evolution during accelerated cooling, and to gain a better control of the final microstructure in an accelerated cooling operation, it is thus necessary to have not only a knowledge of how a particular steel responds to prior thermomechanical processing, but also to be able to accurately predict the transformation onset temperature and the transformation kinetics for any subsequent cooling schedule. This knowledge could then be used in mathematical models to describe the transformation behaviour during a complex cooling operation. Ultimately, knowledge based models of this kind will provide a means for assessing the effectiveness of current cooling practices, and as such, may lead to future refinement of the cooling procedures that are in use today.

This study has been directed towards establishing a method for predicting the onset of the austenite to pearlite decomposition during continuous and non-continuous cooling conditions. The proposed method of analysis is fundamental and can be applied to any cooling situation, regardless of how complex the thermal path may be.

Chapter 2

REVIEW OF THE LITERATURE

2.1 The Onset of the Austenite Decomposition

In 1930, Davenport and Bain^[28] reported their studies on austenite decomposition at a series of constant temperatures. The purpose of the study was to separate the influence of temperature and time on the resultant microstructure. They were the first workers to develop the now familiar time-temperature-transformation (*TTT*), or isothermal transformation diagram as a means of graphically summarising the test results, and to comment on the incubation period which elapses before super-cooled austenite begins to decompose.

Since this pioneering work, others have continued the investigation of isothermal transformations, and today, *TTT* diagrams characterising the start and end of transformation for many steel grades have been compiled.^[29,30,31] Recently, this same approach has been extended to other thermally activated processes, in particular, the precipitation of micro-alloy elements as carbides or nitrides in the technologically advanced High Strength Low Alloy (HSLA) steels.^[32-35]

The fundamental characteristics of the isothermal transformation diagram are important in understanding the microstructural development in a particular steel at various temperatures. The *TTT* diagram can, however, be quantitatively applied to heat treatment only when austenite is made to transform at essentially constant temperatures.

In the practical heat treatment of steels, decomposition of austenite often takes place under non-isothermal conditions rather than at constant temperatures. In 1932, Bain^[36] published a

schematic cooling diagram for a eutectoid plain carbon steel, indicating the curve for the beginning of transformation and the structure produced by several typical cooling rates. This diagram is shown in Figure 2.1.

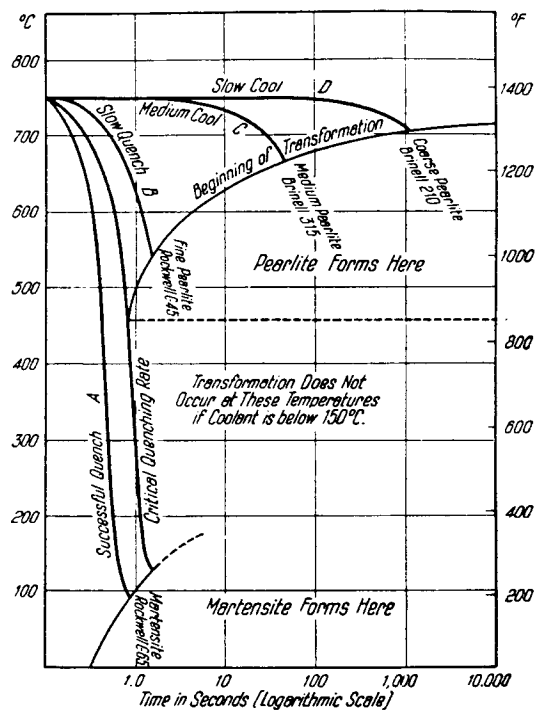


Figure 2.1: An early representation of the relationship between the cooling rate and the transformation start temperature by Bain.^[36]

Subsequently, Davenport^[37] pointed out the need for correlating the transformation during cooling with isothermal data and outlined the principle of a "continuous cooling diagram". However, neither of these researchers offered a practical method of quantitatively correlating the two types of transformation diagrams.

2.2 Inter-Relation of Cooling & Isothermal Transformation Behaviour

A theory, known as the "fractional nucleation" theory, was presented by Scheil,^[38] and independently by Shteinberg,^[39] to predict the onset of transformation under non-isothermal conditions, based on isothermal data. It was proposed that the time spent at a particular temperature, t_i , divided by the isothermal time that is required to start the transformation at that temperature, τ_i , may be considered to represent the fraction of the total incubation (nucleation) time consumed at that temperature.^a Scheil postulated that for a non-isothermal treatment, the transformation will start when the sum of the fractional incubation times equals unity. Mathematically, this may be expressed as:

$$\sum_{i=1}^n \frac{t_i}{\tau_i} = 1 \quad \dots(2.1)$$

where n is the number of incremental steps used in describing the non-isothermal cooling event between the equilibrium temperature and the temperature at which transformation start is observed. Thus, the total time to reach the onset of transformation can be obtained by adding the fractional time increments to reach this stage isothermally, until the sum of the fractions reaches unity. A transformation of this kind is known as an additive reaction. The generalisation of equation (2.1) to any cooling process is thus:

a In this analysis, the pre-transformation time in a *TTT* curve is considered to be the incubation period, also called the transformation nucleation period. The term *incubation* shall be used, since nucleation also refers to the actual transformation event.

$$\int_0^t \frac{dt}{\tau(T)} = 1 \quad \dots(2.2)$$

implying that the process (be it incubation or transformation) will be completed when the sum of the fractional increments of the events reaches unity.

This theory has also been described as the principle of additivity and provides a rational relationship between the transformation at constant temperatures and those that take place under non-isothermal conditions.

There have been a number of attempts to examine the validity of the additivity principle in predicting the cooling transformation from an experimentally determined set of isothermal transformation data. The studies of Manning and Lorig^[40], Jaffe^[41] and Moore^[42] were among the early works which have reference to step quenching (non-continuous cooling) in the thermal treatment of steel.

Manning and Lorig used five steels containing 0.30 wt% C and various amounts of Cr in their studies.^[40] Salt baths were used as a means to maintain isothermal conditions, and the extent of transformation was assessed by quantitative optical microscopy. For a total of 11 isothermal step tests conducted in the "blocky ferrite" range, 5 conformed to the additivity, while the others exhibited a transformation start later than that predicted by additivity. For tests that were first held in the "blocky ferrite" range and then transferred to either the "spear ferrite" or the bainite range, no additive effect was found. They concluded that although the additivity appeared to hold for individual transformation process (eg. austenite to "blocky ferrite" reaction),

it does not apply when a change in morphology (or transformation product) occurs. Thus, the fractional incubation in the bainite region is not additive to previous incubation in the ferrite region because of the difference in the nucleation mode for the two transformation products.

Jaffe^[41] extended the work of Manning and Lorig to examine the conformity of proeutectoid ferrite, bainite and carbide to the additivity principle (described then as the fractional nucleation theory), using SAE 4330 and hypereutectoid steels. He investigated the effect of holding the metastable austenite at one temperature upon its subsequent decomposition at another temperature which was either higher or lower than the previous temperature. Both temperatures were below the stability range of the austenite. From this study, Jaffe concluded that while both the proeutectoid ferrite and carbide transformation are each approximately additive, the bainite transformation is not. This was thought to be because the reaction at high temperatures, e.g. proeutectoid ferrite formation, tends to retard the subsequent transformation to bainite at lower temperatures. On the other hand, holding the sample first in the bainite range did not seem to affect the subsequent transformation to ferrite or cementite.

Reference to both step quenching and inverse step quenching (up quenching) was also made by Moore,^[42] who used a steel containing 0.38 wt% C, 1.63 wt% Ni and 0.98 wt% Cr. Moore examined the validity of the additivity principle with respect to the progress of the transformation. Salt baths were also used in this study to establish the isothermal conditions, and quantitative optical microscopy was employed to assess the progress of the transformation. His results showed that the austenite decomposition process did not always conform to the additivity principle; the transformation generally began when the sum of the fractional incubation (nucleation) times was less than unity.

In 1941, Grange and Keifer^[44] suggested an alternative method for correlating the continuous cooling transformation to its isothermal counterpart. Suppose that a given continuous cooling path crosses the isothermal transformation curve at temperature T_{IT} and time t_{IT} , and later intersects the continuous cooling transformation (CCT) curve at T_{CCT} and time t_{CCT} , as shown in Figure 2.2. They proposed that the two intercepts can be related by the following expression:

$$\tau(T^*) = t_{CCT} - t_{IT} \quad \dots(2.3)$$

where T^* is the mean temperature between T_{CCT} and T_{IT} , i.e.,

$$T^* = \frac{T_{CCT} + T_{IT}}{2} \quad \dots(2.4)$$

Thus, by knowing the t_{IT} versus T_{IT} (the *TTT* curve), and therefore, $\tau = f(T)$, one can iteratively determine t_{CCT} by incrementally changing T_{CCT} until equation (2.3) is satisfied.

This approach assumes that the transformation only begins once the cooling history crosses the isothermal transformation curve, and that the incubation time can be estimated at the mean of the isothermal and the continuous cooling transformation temperatures where the cooling curve crosses both diagrams.

The transformation of austenite to ferrite or pearlite is a thermally activated process; a finite amount of time is necessary for atoms to re-arrange themselves so that they can grow to form a new phase. In order to attain the so-called transformation start condition, nuclei of the new phase must first become stable and then grow to some observable size.

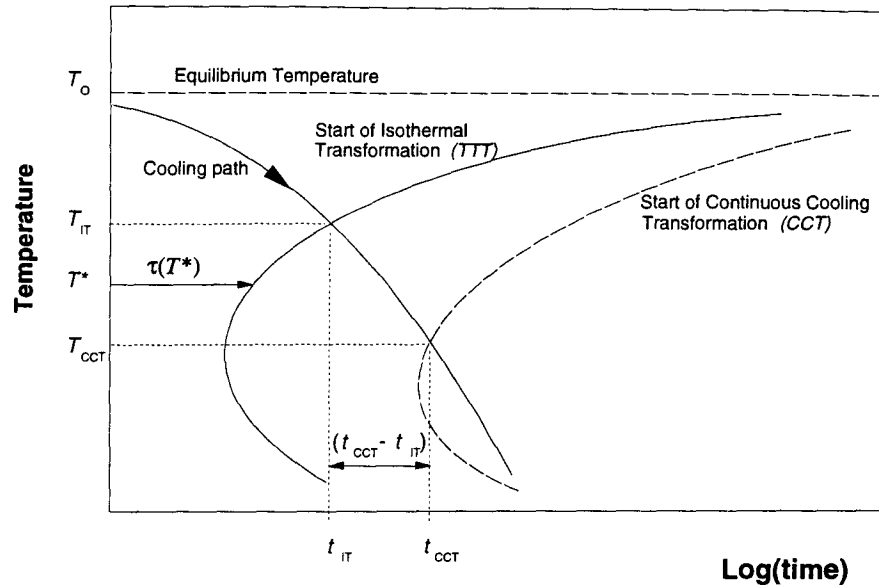


Figure 2.2: Schematic illustration of the Grange-Keifer method of predicting the transformation start under continuous cooling conditions.

Thermodynamically, the pre-transformation clustering processes become possible at temperatures below the equilibrium (Ae_1 or Ae_3 depending on the carbon content) where there is a finite amount of driving force available. Consequently, the incubation process, which encompass clustering (or ordering) and the subsequent growth yielding the transformation start condition, is expected to take place at temperatures below the equilibrium.

2.3 Criteria for the Additivity

Although the additivity principle has had only limited success in predicting the start of transformation, it provides a rational relationship between the transformations that occur under non-isothermal conditions and those that take place at constant temperatures.

Recognising the difficulty in defining the onset of transformation, which is strongly dependent on the method of observation, Cahn^[49] examined the additivity principle with application to the transformation process. His studies led to a criterion for specifying an additive reaction: *whenever the reaction rate is a function of only the instantaneous temperature and the amount transformed, the reaction may be considered additive, i.e.:*

$$\frac{d\chi}{dt} = F(T, \chi) \quad \dots(2.5)$$

where χ is the amount transformed, t and T are the transformation time and temperature, respectively. Christian^[46] generalised this criterion further and found that additivity will also be satisfied if the transformation rate can be described by:

$$\frac{d\chi}{dt} = \frac{G(T)}{H(\chi)} \quad \dots(2.6)$$

where $G(T)$ is a function of the temperature alone and $H(\chi)$ is only a function of the fraction transformed. An additive reaction thus implies that the reaction rate depends solely on the state of the assembly, and not on the thermal path which leads to that state.

Earlier, Avrami^[47] derived the isothermal transformation temperature-time relationships for randomly distributed nuclei, and noted that in the temperature range in which the ratio of the growth rate to the nucleation rate, N/G , is constant, the kinetics of the phase change is independent of the time domain, and hence independent of the thermal path. He referred to this as the "*isokinetic*" range. Under these conditions, the isothermal transformation results can be used to describe phenomena that takes place under conditions of varying temperature.

Cahn^[48] recognised that the isokinetic condition is a very special condition which is not commonly encountered in many transformations. He noted that in many systems nucleation sites are rapidly exhausted early in the reaction and the subsequent transformation process is dominated by growth, which is a temperature dependent parameter. He therefore suggested a more general condition for additivity based on early site saturation.^[48,49]

Based on the assumption that all grains are equally large tetrakaidecahedra (i.e., grains with 14 faces), Cahn^[48] showed that whenever the nucleation rate density (i.e., the number of nuclei per unit volume) is:

$$\begin{aligned}
 \dot{N}_{sfc} &> 6000 \frac{\dot{G}}{D_\gamma^4} \\
 \dot{N}_{edg} &> 1000 \frac{\dot{G}}{D_\gamma^4} \\
 \text{or } \dot{N}_{cm} &> 250 \frac{\dot{G}}{D_\gamma^4} \qquad \dots(2.7)
 \end{aligned}$$

site saturation can be expected to occur early in the reaction, and the subsequent transformation is then essentially governed by growth, which is a temperature dependent parameter. Here the subscripts *sfc*, *edg* and *crn* signify grain surface area, edge length and number of corners, respectively.

He also related these conditions to the time for completion of one half of the transformation, $t_{0.5}$, and found that $t_{0.5}$ for the three types of nucleation is within a factor of 4, regardless of which type is active. That is, the parameter $G t_{0.5}/D_\gamma$ ranges from 0.1 for grain boundary surface nucleation to 0.4 for grain corner nucleation.^[48] He thus concluded that for a reaction where nucleation is confined to grain boundaries (which includes grain boundaries, grain edges and grain corners), the rate of the reaction becomes insensitive to the nucleation rate when:

$$\frac{\dot{G} t_{0.5}}{D_\gamma} < 0.5 \quad \dots(2.8)$$

These criteria can be examined more easily with respect to the transformation process, and consequently, have been critically studied by several workers.^[50-52] However, due to the difficulty in direct experimentation of the incubation process, no successful application of these criteria to incubation has been reported.

2.4 The Incubation Time

The additivity principle provides a mathematical link between the transformations that occur under conditions of varying temperature and those that take place isothermally. Assuming the additivity holds, the ability to predict the transformation behaviour under cooling conditions relies on the accuracy of the data derived at constant temperatures.

The availability of high sensitivity dilatometers, such as that incorporated in the thermomechanical simulation capability of the Gleeble 1500, enables both *TTT* and *CCT* diagrams to be generated readily. The recent application of computer modelling to describe microstructural evolution in metallurgical processes necessitates accurate mathematical description of the transformation diagram, especially when the model is used to examine new processing routes, prior to experimental validation trials. Therefore, representing the available *TTT* (or *CCT*) transformation curves with appropriate mathematical formula, which should reflect physical significance, is one of the current research priorities in process modelling.

2.4.1 Classical Nucleation Theory

According to the linked-flux analysis,^[53,54,55] the transient nucleation rate density can be described as:

$$\dot{N}(t) = \dot{N}_s \exp\left(-\frac{\tau_s}{t}\right) \quad \dots(2.9)$$

$$\dot{N}_s = Z\beta N_0 \exp\left(-\frac{\Delta G^*}{kT}\right) \quad \dots(2.10)$$

where $\dot{N}(t)$ is the transient nucleation rate (nucleation rate as a function of time), \dot{N}_s is the steady state nucleation rate, N_0 is the number of nucleation sites available, τ_s is the induction period for establishing steady state nucleation, Z is the Zeldovich non-equilibrium factor ($\cong 10^{-2}$), β is the rate at which atoms/molecules are attached to the critical nucleus, and k , t & T have their usual meanings.

While the form of the equations for $\dot{N}(t)$ and \dot{N}_s do not change, the parameters τ_s , ΔG^* , β and N_0 are specific to the system and to the type of nucleation process being considered.

Nucleus formation in an isothermal, isobaric system is a thermally activated fluctuation process. It amounts to diffusion (clustering or ordering) over a potential barrier $\Delta G(n)$, which has a maximum at the critical size, n^* , as shown in Figure 2.3. A cluster becomes stable only when it consists of more than n^* atoms and its energy is kT units less than ΔG^* . Small cluster will have a substantial chance of decomposing. The region Δn , bounded by $(\Delta G^* - kT)$, is essentially flat so that cluster will move by "random walk" in this interval.

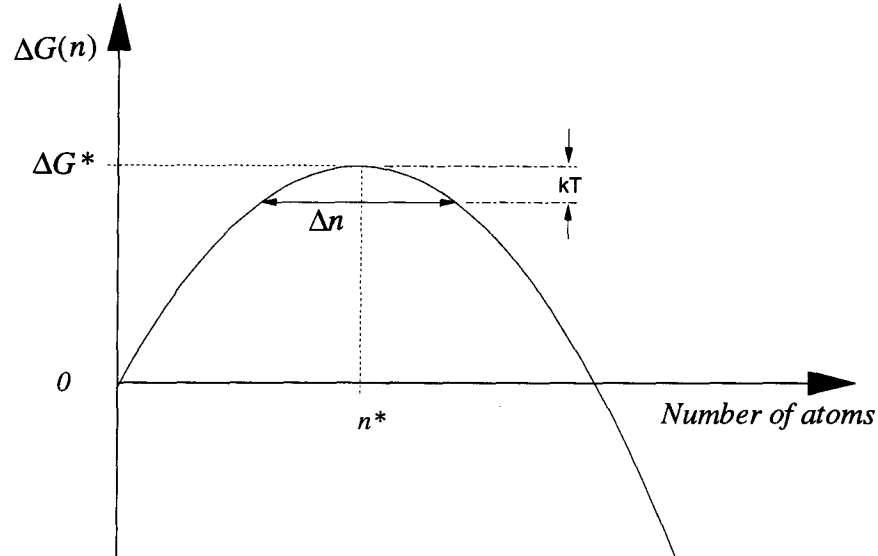


Figure 2.3: Free energy of cluster (pre-nucleation) formation.

Based on the principle of *time reversal*^b, Russell^[53] derived an expression for the time for a nucleus to form or decompose, t_r :

$$t_r = \frac{(\Delta n)^2}{2\beta} + \int_1^{(n^* - \frac{\Delta n}{2})} \left\{ \frac{kT}{\beta_n} \left(\frac{\delta \Delta G}{\delta n} \right)^{-1} \right\} dn \quad \dots(2.11)$$

where the first term on the right hand side corresponds to the time needed for a cluster to "randomly walk" to change the number of atoms by Δn , and the second term represents the

b That is, fluctuations on average arise and decay in the same way. In other words, nucleus formation takes place by the same mechanism and in the same length of time as nucleus decay.

time required to change from the monomer (i.e., a cluster of 1 atom) to a cluster of $n^* - \Delta n/2$ atoms. This time, t_r , was suggested to be a measure of the incubation time that is necessary for establishing steady state nucleation, i.e., the same as τ_s in equation (2.9).

By considering grain boundary nucleation, expressions for the incubation time to establish steady state grain boundary nucleation, τ_s , were also derived for various type of cluster geometries,^[53] which share a general form:

$$\tau_s \propto \frac{T}{(\Delta G_v)^m D_{eff}} \quad \dots(2.12)$$

where T , ΔG_v and D_{eff} are the temperature, the volume free energy change associated with nucleus formation and the effective diffusivity, respectively. Thus, the rate of establishing the steady state nucleation condition, ν_s , is:

$$\nu_s \propto \frac{(\Delta G_v)^m D_{eff}}{T} \quad \dots(2.13)$$

That is, ν_s is proportional to the product of the driving force, $(\Delta G_v)^m$, and the mobility, D_{eff} .

The exponent m is a constant and is a characteristic of the nucleation mode. Russell^[53] considered the nucleation of precipitates along the grain boundaries and found $m = 2$ for coherent precipitate, whose formation is controlled by volume diffusion. If the nucleus is incoherent and formed by the diffusion of solute along the grain boundaries, he found $m = 3$.

The change in volume free energy, ΔG_v , associated with austenite decomposition becomes finite and increases in magnitude as temperature decreases below the equilibrium temperature.^[56] On the other hand, the diffusion coefficient, D , depends on the temperature through an Arrhenius-type equation:^[57]

$$D = D_0 \exp\left\{-\frac{Q}{RT}\right\} \quad \dots(2.14)$$

where D_0 is the pre-exponential constant, Q is the activation energy for diffusion. The magnitude of D decreases as the temperature is lowered.

When the amount of undercooling is small (i.e., at temperatures just below the equilibrium temperature), the amount of free energy available to drive the decomposition process, ΔG_v , is small. Thus, despite the atoms being very mobile at this higher temperature, the decomposition process is expected to be sluggish; long incubation times are predicted according to equation (2.12). While at a low temperature, a large amounts of free energy is available to promote the decomposition process. However, the process is limited by the slow mobility of the atoms (i.e., small value of D), and hence, a longer time is needed for the reaction to take place.

At some intermediate temperature, there is an optimal product of ΔG_v and D , which results in the fastest rate for establishing the steady state nucleation condition, and hence, the shortest time to complete the incubation event, from equation (2.12). Thus, equation

(2.12) predicts a "C" curve "transformation start" dependency which is the characteristic behaviour of diffusion controlled transformations, and is observed for the isothermal decomposition of austenite to ferrite or pearlite.

However, evaluation of ΔG_v and D_{eff} for practical steel chemistries requires detailed studies of the alloy interactions and the effect that each element has on the activity and mobility of all elements present in the steel. This is a subject of research in its own right^[58-60] and is beyond the scope of the current study.

2.4.2 The Growth Equation

The austenite to pearlite transformation, as occurs in eutectoid (or near eutectoid) steel under slow cooling conditions and in hypoeutectoid steel at higher cooling rates, is emphasized in this research. In 1946, Zener^[61] reported his studies on the kinetics of pearlite growth in the austenite decomposition process, and formalised a mathematical expression for the rate of growth of pearlite lamellar as a function of carbon content and the diffusivity of carbon (solute atoms) in austenite, ahead of the growing pearlite:

$$v_p = \frac{(C_{\alpha/\gamma}^* - C_{Fe_3C/\gamma}^*)}{(C_{Fe_3C} - C_{Fe_3C/\gamma}^*)} \left\{ \frac{D}{l} \right\} \quad \dots(2.15)$$

where $C_{\alpha/\gamma}^*$ and $C_{Fe_3C/\gamma}^*$ are the interfacial composition of carbon just ahead of the ferrite and cementite lamellar, respectively (as shown in Figure 2.4), $(C_{Fe_3C} - C_{Fe_3C/\gamma}^*)$ is the composition difference across the cementite and austenite interface, D is the diffusion coefficient for carbon in austenite and l is the effective diffusion distance.

The effective diffusion distance which is the mean distance of lateral transport of the carbon from in front of the growing ferrite lamella to in front of the growing cementite, and is therefore, a function of the inter-lamellar spacing of the pearlite and the interface curvature, is inversely proportional to the degree of undercooling, ΔT .^[64]

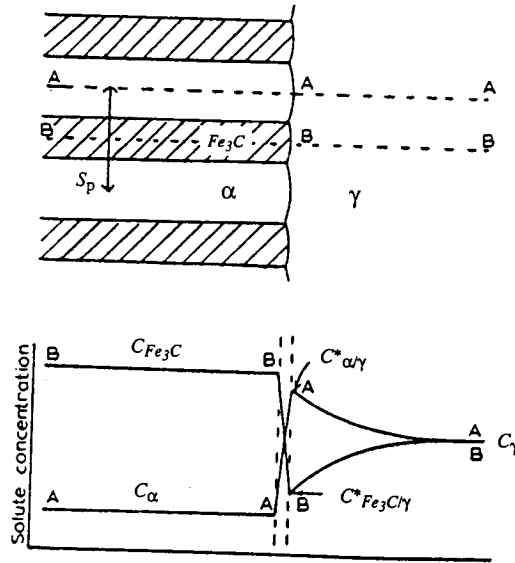


Figure 2.4: Schematic composition profile across the pearlite lamella and austenite interface.

Zener assumes that the redistribution of solute atoms (interstitial carbon atoms) ahead of the lamellar front, which leads to the growth of pearlite, takes place inside the austenite grain (i.e., by volume diffusion). Under these circumstances, the composition driving force, $\Delta C = (C_{\alpha/\gamma}^* - C_{Fe_3C/\gamma}^*)$, is approximately proportional to the degree of undercooling, ΔT .

The dependence of diffusivity on temperature is described in the Arrhenius equation (equation (2.14)). Given that ΔC is proportional to ΔT , equation (2.15) can be rearranged to express the growth rate in terms of undercooling and temperature as follows:

$$v_p \propto (\Delta T)^2 \exp\left(-\frac{Q}{RT}\right) \quad \dots(2.16)$$

where Q is the activation energy for diffusion, R is the gas constant and T is the absolute temperature.

Since the growing pearlite nodule does not change the carbon concentration of the austenite remote from the growing interface, neighbouring pearlite nodules do not influence each other until they impinge upon one another. The growth rate can therefore be assumed constant at a given temperature.

When the boundary of the austenite grain becomes covered with nuclei, a condition described as site saturation, the isothermal time for establishing a certain fraction of pearlite is then:

$$\tau_G \propto \frac{1}{v_p} \quad \dots(2.17)$$

$$\propto (\Delta T)^{-2} \exp\left(\frac{Q}{RT}\right) \quad \dots(2.18)$$

Using a value of 36 *kCal/mole* for the activation of carbon in austenite, Zener^[61] noted that equation (2.18) exhibits a "C" curve behaviour which is characteristic of the *TTT* diagram.

Although, Fisher,^[62] Turnbull^[63] and Hillert^[64] refined and generalised Zener's theory, the dependence of the growth time, τ_G , on the degree of undercooling and temperature shares the general form described in equations (2.17) and (2.18), with the exception of the inclusion of an exponent m for the supercooling term, ΔT :

$$\tau_G \propto (\Delta T)^{-m} \exp\left(\frac{Q}{RT}\right) \quad \dots(2.19)$$

where m is a constant and reflects the mode of diffusion that leads to the growth of the new phase. This generalisation was incorporated to account for different modes of diffusion of solute.

2.5 Contemporary Approaches

The introduction of mathematical modelling to describe metallurgical processes, in particular, to quantify the microstructure evolution during thermal or thermomechanical treatment has become increasingly important in the steel industry as a tool for optimising the processing conditions.

Modelling of microstructure evolution during cooling has frequently involved the use of the Avrami equation, which has the form:

$$\chi = 1 - \exp\{-b(T)t^n\} \quad \dots(2.20)$$

where χ is the fraction transformed in time t , b and n are empirically determined constants. This equation has been used to satisfactorily characterise the extent of the isothermal decomposition of austenite to ferrite, pearlite or bainite in a number of studies.^[65-71]

Recognising the simplicity of the additivity principle, several recent studies have combined it with the Avrami equation so that the isothermal kinetic data can be used to estimate the onset of the transformation under continuous cooling conditions.

In 1981, Umemoto and co-workers^[72] introduced the concept of the "equivalent cooling curve". The concept assumes the transformation is additive, i.e., it obeys Scheil's rule (equations 2.1 & 2.2) and simultaneously that the isothermal transformation can be characterised by the Avrami equation. An expression for the equivalent time, t_{eq} , to reach a fraction χ was then obtained, which has the form:

$$t_{eq} = \frac{1}{[b(T_x)]^{1/n}} \int_{T_x}^{T_0} \left\{ \frac{[b(T^*)]^{1/n}}{\dot{\theta}(T^*)} \right\} dT^* \quad \dots(2.21)$$

where the integral is evaluated along the cooling path and, hence, represents the non-isothermal contribution. The equation shows that the fraction transformed by cooling from the equilibrium temperature T_0 to T_x with a cooling rate $\dot{\theta}$, is equal to that obtained by isothermally holding the sample at T_x for an equivalent period t_{eq} .

Equivalent cooling curves, which are determined from isothermal transformation kinetics together with a specific thermal history, are suggested to be an alternative to the *TTT* diagram. It is claimed that equivalent cooling curves would provide better accuracy in predicting the transformation behaviour for a given non-isothermal cooling history.^[72]

While this concept was developed to describe the cooling transformation kinetics, based on the isothermal kinetic data with an assumption that the reaction is additive, there is also a possibility that it could be used to determine the start of transformation, $\chi=0.1\%$, for the *TTT* curve.

However, such extrapolation should be used with caution as Hawbolt *et. al.*^[65,66] have shown that the incubation and the growth of a new phase are two separate events in a transformation process. While the growth of pearlite from the austenite matrix is additive and can be characterised by the Avrami equation, the incubation of pearlite formation in the same steel does not necessary conform to additivity conditions.^[65] Therefore, extrapolation of the equivalent cooling curve to approximate the start of transformation could lead to misleading

results.

Recognising the difficulty in obtaining experimental isothermal transformation data, in particular, definitively characterising the onset of the decomposition, especially for low alloyed steels, Gergely and co-workers^[73] presented a method for deriving the isothermal transformation diagram from measurements obtained under continuous cooling conditions. This technique also assumes that the transformation event, both incubation and growth processes, can be described empirically by an Avrami-type equation of the form:

$$\chi = 1 - \exp\{-(kt)^n\} \quad \dots(2.22)$$

where $k^n = b$ in equation (2.20).

From the measured transformed fraction and the transformation rate at any temperature, both coefficients k and n can be simultaneously calculated. A multi-parameter analysis was then used to derive the mean values of k and n at each temperature^[73] and the corresponding loci of the 1% and 99% transformation lines were drawn on the temperature-time plot.^[73,74] The time exponent n , obtained by this technique is highly sensitive to temperature; at 720°C n has a value of 10.45 and decreases to 4.28 at 600°C.^[73] However, the composition of the steel concerned was not mentioned in the article.

According to Kuban *et. al.*,^[51] Avrami's equation will satisfy the additivity principle, as defined by Christian^[46] (Section 2.3), if and only if the exponent n is a constant, independent of temperature, and the rate constant k (or b in equation (2.20)) is a function only of the transformation temperature.

In 1977, Kirkaldy and colleagues^[76] presented a thermodynamic derivation for calculating the equilibrium transformation temperature for the onset of the austenite \rightarrow ferrite ($\gamma \rightarrow \alpha$) transformation, i.e., A_{e_3} , based on steel chemistry. The concept proved to be versatile and capable of handling a wide range of steel compositions.^[77] They also extended their studies to predict the isothermal time to attain 0.1% transformation assuming instantaneous site saturation occurred, and subsequent diffusion controlled growth for the $\gamma \rightarrow \alpha$ transformation. This approach assumes that the previously described incubation period (the pre- 0.1% transformation region) is a region of slow growth. Their derivation began with the modified Zener growth equation^[61] of the form:

$$v \propto (\Delta T)^m \exp\left(-\frac{Q}{RT}\right) \quad \dots(2.24)$$

where ΔT is the degree of undercooling, i.e., $(A_{e_3} - T)$; Q is the activation energy for diffusion in austenite and m is a constant relating to the mode of diffusion (diffusion path). A value of 3 for m was chosen as "the best average representation over all",^[76] it was suggested that any error introduced by such a choice could be empirically accommodated in the regression of the effective activation energy for diffusion. The effects of alloying elements and austenite grain size were absorbed in the proportionality constant.

Regression over a set of *TTT* diagrams for more than 20 hypoeutectoid steels yielded an expression for the isothermal time to attain 0.1% ferrite from austenite of the form:

$$\tau_{0.1\%} = \frac{\exp\left(\frac{20\text{kCal/mol}}{RT}\right)}{2^{N/8}(Ae_3 - T)^3} (60C + 90Si + 160Cr + 200Mo) \quad \dots(2.25)$$

where N is the ASTM grain size number, and the compositions are in wt%.

The success of equation (2.25) in describing the isothermal onset of ferrite formation (0.1%), i.e., the "start time" for the TTT curves for medium and low alloy steels is quite remarkable. However, for high carbon and heavily alloyed steels, the equation could not retrace the experimental curves.^[78,79]

The subsequent prediction of the start of transformation for the CCT curve, using the Scheil summation method, was also carried out; but predicted CCT curve did not agree well with the experimental data.^[78,79] As a consequence, the expression for the incubation time for ferrite was revised, and similar expressions for pearlite and bainite were also developed,^[79] which enable them to generate TTT diagram for several product phases. This approach is still limited to low alloyed steels.

In 1977, Shimizu and Tamura^[81] pointed out that if the cooling rate does not remain continuous during cooling, the non-isothermal transformation start temperature can be significantly different from that predicted by the "conventional" CCT curve; the latter is commonly generated by either Newtonian or linear cooling. They also indicated that the experimentally generated TTT curve is dependent on the initial transient cooling rate used to reach the isothermal temperature.

A solution to the inverse of additivity that would enable the isothermal incubation time to be derived directly from the continuous cooling data, was recognised by Kirkaldy and Sharma.^[80] The approach was demonstrated first by inversion of a published *CCT* curve to a *TTT* curve, which was then used to forward predict a *CCT* curve for Jominy cooling conditions. However, the procedure assumes that the *CCT* curve was obtained from a set of linear cooling experiments in which all cooling rates used in the generation of a *CCT* curve were constants, independent of the sample temperature. There was no experimental verification presented.

Recently, the consequences of the additivity rule with respect to incubation were further pointed out by Wierszyllowski.^[82] He showed that in all experiments conducted to generate *TTT* curves, there was a finite amount of incubation fraction being consumed in cooling the specimen to the isothermal test temperature. He also suggested a method for direct measurement of the true isothermal incubation that would theoretically validate the use of Scheil's summation. However, there has been no verification conducted experimentally.

Chapter 3

OBJECTIVES AND SCOPE OF THE STUDY

The significance of accurately predicting the onset of transformation in understanding the microstructure evolution during cooling has long been recognised. Despite the considerable amount of research and development which has been conducted to establish a method for estimating the onset of the austenite decomposition, the prediction methods available today^[13,15,24] are still somewhat semi-empirical. Their applications are limited to continuous cooling situations in which the cooling rate does not change drastically and have not been experimentally verified.

Although *CCT* diagrams have long been used to evaluate the metallurgical response of different steels, one must be aware that most *CCT* diagrams are constructed from tests with natural or linear cooling situations. This restricts their applicability to processes involving comparable cooling conditions. Modern steel processing conditions can become quite sophisticated involving a range of continuous and step cooling situations;^[25-27] *CCT* diagrams appropriate to these more complex processes would have to be generated using comparable cooling conditions.

The additivity principle provides a possible mathematical relationship between the transformations that occur under non-isothermal conditions and those that occur at constant temperatures. As such, it offers a potential procedure for using isothermal data to describe a process involving a complex thermal path.

However, the success of the additivity principle in estimating the transformation start has not been rigidly tested. Thus, the objective of this study is to gain a better understanding of the additivity principle and its applicability to the incubation and transformations involved in the decomposition of austenite to pearlite.

To fulfil this objective, the scope of this study will encompass the following tasks:

- i)* The relationship between the isothermal and cooling transformation start diagrams, with respect to Scheil's additivity rule, shall be critically re-examined to gain further understanding of the consequences and implications of the additivity .

An "ideal" *TTT* curve, which would satisfy the use of Scheil's equation (equation 2.1 & 2.2) in predicting the start of transformation in non-isothermal conditions, will be introduced. Mathematical relationships between the experimental time to the start of transformation and the ideal incubation time shall be derived, and methods for obtaining the ideal *TTT* curve from cooling data will also be established.

- ii)* The start of transformation from austenite to pearlite will be experimentally measured using the Gleeble 1500 under isothermal (*TTT*), continuous cooling (*CCT*) and non-continuous cooling conditions for a eutectoid steel.

- iii)* An "ideal" *TTT* curve for the eutectoid steel will be derived using the controlled cooling data. The derived "ideal" *TTT* curve will be employed in the Scheil equation to predict the continuous cooling behaviour, and the results compared with the experimental measurements.
- iv)* The prediction capability of the Scheil additivity principle will be tested against the conventional methods for estimating the transformation start temperature.
- v)* Simulation of the actual cooling schedules from a BHP rolling mill, typifying a semi-continuous cooling condition, will also be conducted and the result obtained shall be used for the assessment.

Chapter 4


INCUBATION TIME AND THE ADDITIVITY PRINCIPLE

Theoretically, an isothermal transformation diagram is unique to a steel with a particular solution treatment history; the austenite decomposition kinetics depend only on the composition and the grain size prior to transformation. The additivity principle offers a mathematical relationship between non-isothermal events and their isothermal counterpart.

The isothermal data, which are generated by experiments, inherently contain an initial temperature transient which arises prior to attaining the isothermal decomposition conditions. The transient exists, at least in part, within the decomposition range. Thus, the "isothermal" nature of the experimental data depends on the relative proportion of the event that takes place at the desired temperature and that which happens during the initial cooling transient. For many steels, particularly the plain low carbon steels, the transformation incubation times near the "nose" temperature (i.e., the temperature at which the decomposition kinetics are most rapid) are very short, which makes it difficult to obtain isothermal data that is meaningful.

Dec. 16, 1991

Readers of this thesis, particularly the development of the ideal isothermal transformation curve on pages 34 to 44, are directed to the seminal paper by I.A. Wierszyllowski, "The Effect of Thermal Path to Reach Isothermal Temperature on Transformation Kinetics", Met. Trans., 22A, 1991, pp993-999.



Dr. E.B. Hawbolt

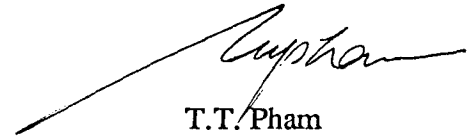
Professor
Metals and Materials Engineering

NOTICE TO THE READER

Intending readers of this thesis, particularly the development of the ideal isothermal transformation curve on pages 34 to 44, are directed to the seminal paper by I. A. Wierszylloski [1].

The attention of readers is drawn also to the following published discussion and response:

- (a) 'Discussion of "Predicting the Onset of Transformation under Noncontinuous Cooling Conditions: Part I. Theory" and "Predicting the Onset of Transformation under Noncontinuous Cooling Conditions: Part II. Application to the Austenite Pearlite Transformation"' by I.A. Wierszylloski [2]; and
- (b) Authors' Reply by T.T. Pham, E.B. Hawbolt and J.K. Brimacombe. [3]



T.T. Pham

-
- [1] *Metall. Mater. Trans. A* 1991, vol. 22A, pp 993-99.
 - [2] *Metall. Mater. Trans. A* 1997, vol. 28A, p. 251.
 - [3] *Metall. Mater. Trans. A* 1997, vol. 28A, p. 1089.

4.1 The "Ideal" *TTT* Curve for the Incubation

Suppose for a steel with given composition and austenite grain size, there exists an "ideal" *TTT* curve for the start of transformation from austenite to pearlite, such that it satisfies the Scheil equation (equation 2.1 & 2.2) for predicting the start of transformation under non-isothermal conditions. This *TTT* curve could only be generated with an infinitely rapid initial cooling rate to each isothermal temperature.

Wierszylowski,^[82] ascribing the pre-transformation region in terms of incubation, pointed out that there was a finite amount of incubation being consumed during the initial transient cooling to the test temperature, T_i , in accordance with Scheil's theory.^[82] Figure 4.1 is a schematic illustration of a typical thermal path employed in determining the isothermal incubation time at temperature T_i . The resulting *TTT* curve obtained in this way is called an "experimental" *TTT* curve and is shown as a solid curve. Included in this Figure is an "ideal" *TTT* curve, shown as a dash curve, to illustrate the relationship between the experimental and ideal *TTT* curves. Since the experimentally generated *TTT* curve incorporates a measurable initial cooling transient to the isothermal temperature, it is displaced to the longer times relative to the "ideal" *TTT* curve.

Let $\tau(T)$ be a mathematical function which describes the shape of the ideal *TTT* curve. Thus, we can quantify the relationship between the experimental and ideal times according to the Scheil equation (equation 2.1 & 2.2). Assuming the thermal path from the equilibrium temperature to the intercept of the experimental *TTT* curve consists of n isothermal segments.

Application of Scheil's equation yields:

$$\sum_{i=1}^n \frac{\Delta t_i}{\tau(T_i)} = 1 \quad \dots(4.1)$$

$$\sum_{i=1}^{(n-1)} \frac{\Delta t_i}{\tau(T_i)} + \frac{(t_s - t_c)}{\tau(T_t)} = 1 \quad \dots(4.2)$$

where Δt_i are the incremental time steps. The first term on the left hand side of equation (4.2) represents the summation along the cooling path; while the second term is the fractional incubation time consumed due to the isothermal holding at temperature T_t .

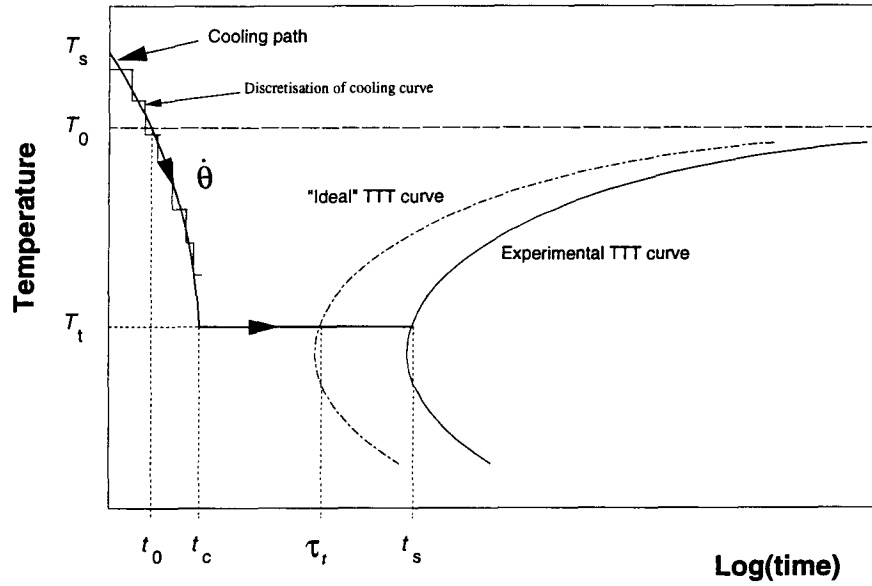


Figure 4.1: Schematic illustration of the relationship between the "ideal" and experimental incubation time at temperature T_t .

To better approximate the initial transient cooling path, we can reduce the time increments such that the summation can be transformed mathematically to become:

$$\int_{t_0}^{t_c} \frac{dt}{\tau(T)} + \frac{(t_s - t_c)}{\tau(T_i)} = 1 \quad \dots(4.3)$$

Since $\tau(T)$ is a function of temperature, we may desire to transform the limits of integration from $t_o \rightarrow t_c$ to $T_o \rightarrow T_i$ as follows:

$$\int_{t=t_0}^{t=t_c} \frac{1}{\tau(T)} \left(\frac{dt}{dT} \right) dT + \frac{(t_s - t_c)}{\tau(T_i)} = 1 \quad \dots(4.4)$$

$$\int_{T_0}^{T_i} \frac{1}{\tau(T)} \left(\frac{dT}{dt} \right) dT + \frac{(t_s - t_c)}{\tau(T_i)} = 1 \quad \dots(4.5)$$

or:

$$\int_{T_i}^{T_0} \frac{dT}{\tau(T)\dot{\theta}(T)} + \frac{(t_s - t_c)}{\tau(T_i)} = 1 \quad \dots(4.6)$$

where T_0 is the temperature at which the sample becomes unstable relative to the transformation event, $\dot{\theta}$ is the cooling rate and defined as $-dT/dt$, τ is the isothermal incubation time and is a function of temperature and τ_i is the incubation time at T_i . This integration of the consumption of fractional incubation time (equation 4.6) can be rearranged in terms of t_i to yield:

4.1 The "Ideal" TTT Curve for the Incubation

$$t_s = t_c + \tau_t \left\{ 1 - \int_{T_i}^{T_0} \frac{dT}{\tau(T)\dot{\theta}(T)} \right\} \quad \dots(4.7)$$

The total cooling time, t_c , may be evaluated by integrating the cooling rate with respect to the temperature changes along the cooling path, i.e.:

$$t_c = \int_{T_s}^{T_i} \frac{dT}{-\dot{\theta}(T)}$$

or:

$$t_c = t_0 + \int_{T_i}^{T_0} \frac{dT}{\dot{\theta}(T)} \quad \dots(4.8)$$

Substituting (4.8) into (4.7) results in the following:

$$t_s = \tau_t + t_0 + \int_{T_i}^{T_0} \left[1 - \frac{\tau_t}{\tau(T)} \right] \frac{dT}{\dot{\theta}(T)}$$

or:

$$(t_s - t_0) = \tau_t + \int_{T_i}^{T_0} \left[1 - \frac{\tau_t}{\tau(T)} \right] \frac{dT}{\dot{\theta}(T)} \quad \dots(4.9)$$

If the time, t_0 , to reach the isothermal transformation phase boundary temperature T_0 is very short compared to the observed transformation start time, t_s , which typically is the case, then equation (4.9) becomes:

$$t_s \approx \tau_i + \int_{T_i}^{T_0} \left[1 - \frac{\tau_i}{\tau(T)} \right] \frac{dT}{\dot{\theta}(T)} \quad \dots(4.10)$$

For isothermal tests conducted above the nose temperature of the *C* curve, it follows that $\tau(T) \geq \tau_i$ in the temperature range from T_0 down to T_i . Thus, the integral on the right hand side of equation (4.10) remains positive. Consequently, it means that the experimental isothermal start time, t_s , is always longer than the ideal incubation time, τ_i , at the test temperature by an amount represented by the integral on the right hand side of equation (4.10). Obviously, when the initial cooling rate is very rapid the integrand becomes negligible, in which case the experimental start time may be taken to be the isothermal incubation time. This is in accordance with our definition of the ideal incubation time, as the experimental incubation time will approach the ideal incubation time when the initial cooling is instantaneous.

In fact, Shimizu & Tamura^[81] pointed out that since the experimental isothermal start time depends on the initial cooling rate, experimental *TTT* curves varied, depending on the experimental procedure used to obtain the isothermal results. For this reason, they no longer represent a truly unique isothermal transformation diagram.

The influence of the initial cooling on the experimental *TTT* curve can be explained with the aid of Figure 4.2. Consider a particular cooling rate, $\dot{\theta}_1$, is obtained in transferring a specimen to the isothermal test temperature. Suppose that this cooling rate is slower than the critical rate, and if the specimen is allowed to continue cooling at this rate, transformation will eventually start at temperature T_1 , where it intercepts a *CCT* curve.

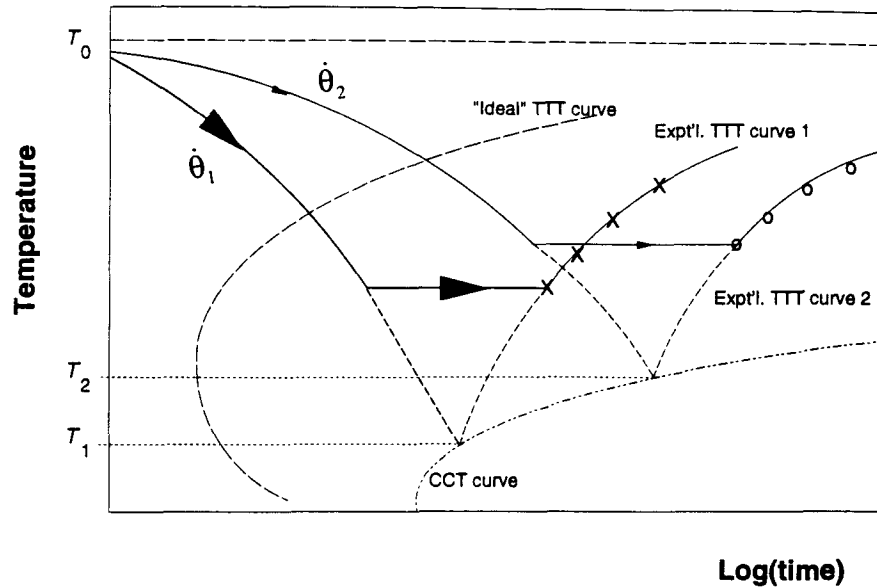


Figure 4.2: Interrelationship between the continuous cooling, experimental and "ideal" isothermal starting time.^a

However, isothermal tests are conducted at temperatures higher than T_1 to produce a *TTT* curve (curve 1). When this *TTT* curve is extrapolated to lower temperatures, it will eventually intersect the *CCT* curve at T_1 . Similarly, if another experimental procedure is used, which yields an initial cooling rate $\dot{\theta}_2$ in transferring a specimen to the isothermal test temperatures, a different *TTT* curve (curve 2) will result. Thus, the only unique *TTT* curve is that obtained by using an infinite cooling rate to attain the isothermal test temperature, i.e., an "ideal" *TTT* curve.

^a The relative spacing between the "ideal" and the experimental transformation start curve is exaggerated for illustration only.

4.1.1 Measurement of The "Ideal" Incubation Time

Equation (4.10) offers a quantitative relationship between the experimentally measured isothermal start time and the true incubation time of a steel, based on Scheil's additivity rule. However, since $\tau(T)$ is not known, nor is τ_i , the integral cannot be evaluated directly.

Theoretically, τ_i is constant while t_i is dependent on the cooling rate used to reach the test temperature, T_i . If a sample was cooled at a constant rate of $\dot{\theta}_{CI}$ to the test temperature T_i , and the corresponding start time was measured to be t_{sI} , equation (4.10) would reduce to:

$$t_{sI} \approx \tau_i + \frac{1}{\dot{\theta}_{CI}} \int_{T_i}^{T_0} \left[1 - \frac{\tau_i}{\tau(T)} \right] dT$$

or:

$$\dot{\theta}_{CI} t_{sI} \approx \dot{\theta}_{CI} \tau_i + \int_{T_i}^{T_0} \left[1 - \frac{\tau_i}{\tau(T)} \right] dT \quad \dots(4.11)$$

Alternatively, if another cooling rate, $\dot{\theta}_{C2}$, was also used to reach T_i and correspondingly the start time was measured to be t_{s2} , we would have:

$$\dot{\theta}_{C2} t_{s2} \approx \dot{\theta}_{C2} \tau_i + \int_{T_i}^{T_0} \left[1 - \frac{\tau_i}{\tau(T)} \right] dT \quad \dots(4.12)$$

These two cooling conditions are schematically illustrated in Figure 4.3.

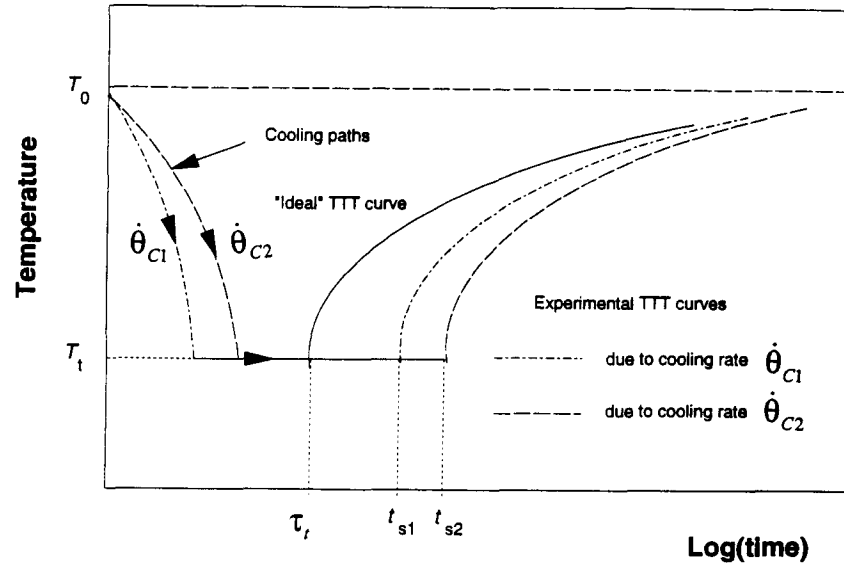


Figure 4.3: Schematic illustration of the relationship between the "ideal" and experimental incubation time.^b

The integrals which appear in both equations (4.11) and (4.12) are, in fact, identical since they are evaluated from T_0 to T_i and do not involve the time variable; they are independent of the thermal path. Hence, subtracting equations (4.12) from (4.11) will lead to the following result:

$$\tau_i \approx \frac{(\dot{\theta}_{C1}t_{s1} - \dot{\theta}_{C2}t_{s2})}{(\dot{\theta}_{C1} - \dot{\theta}_{C2})} \quad \dots(4.13)$$

b The relative spacing between the "ideal" and the experimental transformation start curve is exaggerated for illustration only.

where all quantities on the right hand side are measurable enabling τ_i to be determined directly from the experimental data.

4.2 Calculation of The "Ideal" Incubation Time from Cooling Data

Assuming the Scheil equation can use isothermal data to predict continuous cooling transformation events, an "ideal" *TTT* curve can be determined from the transformation results which are associated with a range of known cooling conditions.

For a constant cooling rate, the Scheil equation (equation (2.2)) can be transformed to the form similar to equation (4.6):

$$-\int_{T_0}^{T_{CCT}} \frac{1}{\tau(T)} \frac{1}{\dot{\theta}(T)} dT = 1 \quad \dots(4.14)$$

where the cooling rate $\dot{\theta}$ is negative, as is the temperature increment, dT .

Since the formation of the new phase is only possible at temperatures below the equilibrium transformation temperature, which is a characteristic of the steel chemistry, the integration is meaningful only at temperatures below the equilibrium decomposition temperature; the transformation then occurs for a given degree of undercooling, ΔT . It should be emphasized that above the equilibrium temperature, decomposition is not possible and, hence $\tau(T)$ is infinite.

Thus, transforming equation (4.14) to integrate over ΔT yields:

$$\int_0^{\Delta T_{CCT}} \frac{1}{\tau(\Delta T)} \frac{1}{\dot{\theta}(\Delta T)} d(\Delta T) = 1 \quad \dots(4.15)$$

where the degree of undercooling, ΔT , is defined as $T_0 - T$. ΔT_{CCT} is the total amount of undercooling to attain the start of transformation.

Consider the cooling condition in which the cooling rate is constant, $\dot{\theta}_C$. Equation (4.15) simplifies to:

$$\int_0^{\Delta T_{CCT}} \frac{1}{\tau(\Delta T)} d(\Delta T) = \dot{\theta}_C \quad \dots(4.16)$$

Differentiating equation (4.16) with respect to the degree of undercooling, ΔT , an expression is obtained for τ in terms of the cooling rate and the degree of undercooling as follows:

$$\frac{1}{\tau(\Delta T)} = \frac{d(\dot{\theta}_C)}{d(\Delta T_{CCT})} \quad \dots(4.17)$$

where ΔT_{CCT} is the magnitude of the undercooling at which the transformation of the new phase begins on cooling.

4.2 Calculation of The "Ideal" Incubation Time from Cooling Data

Thus, by knowing the cooling rate that the steel has experienced below the equilibrium temperature and the temperature at which the transformation begins, one can estimate the ideal isothermal incubation time, and therefore construct the ideal *TTT* curve.

Chapter 5

EXPERIMENTAL DESIGN

5.1 Materials

All experiments were conducted using an industrial eutectoid carbon steel having the composition shown in Table 5.1. The eutectoid grade was chosen because of its inherent high hardenability, which enables the experimental study of incubation time to be conducted.

Table 5.1: Composition of steel used in this study.

Elements:	<i>C</i>	<i>Mn</i>	<i>Si</i>	<i>P</i>	<i>S</i>	<i>Al</i>	<i>Cr</i>	<i>Ni</i>
Wt%:	0.82	0.88	0.28	0.015	0.008	0.001	0.032	0.006

The temperature for the onset of austenite formation from pearlite on heating, A_{C1} , was calculated for this steel to be 722 °C.^[84] A more detailed thermodynamic calculation of the equilibrium temperature, A_{e1} , according to Kirkaldy,^[76] yielded 721 °C, and the corresponding eutectoid composition of 0.71 wt%C. Although this indicates that the steel is hyper-eutectoid, the maximum amount of cementite, Fe_3C , expected to form by lever rule calculation is less than 2%.

Thermodynamically based equations reported by Kirkaldy,^[76] were also employed to determine the composition boundaries of the $Fe(X)$ - C phase fields (where X is the combination of alloying elements other than carbon). The resulting binary phase diagram for the steel used in this study is shown in Figure 5.1. From this diagram, the steel intersects the γ/Fe_3C phase

boundary, i.e., A_{Cm} , at 768 °C.

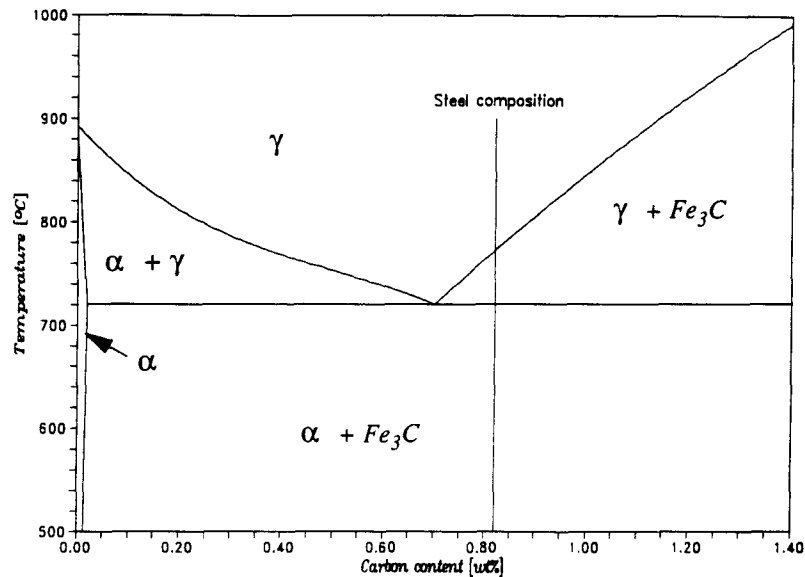


Figure 5.1: The modified $Fe(X)$ -C phase diagram for the eutectoid steel having the composition shown in Table 5.1.

In order to minimise the compositional variation that might exist between, and within each specimen, the as-received steel rod was homogenised in evacuated quartz tube at 1100°C for 14 hours. The steel rod was then annealed at 850 °C for 30 minutes and furnace cooled to room temperature to reduce the austenite grain size and restore the ductility of the room temperature microstructure for subsequent machining operations. This heat treatment sequence yielded an average Vicker hardness of 267, and a microstructure consists predominantly of pearlite as shown in Figure 5.2.

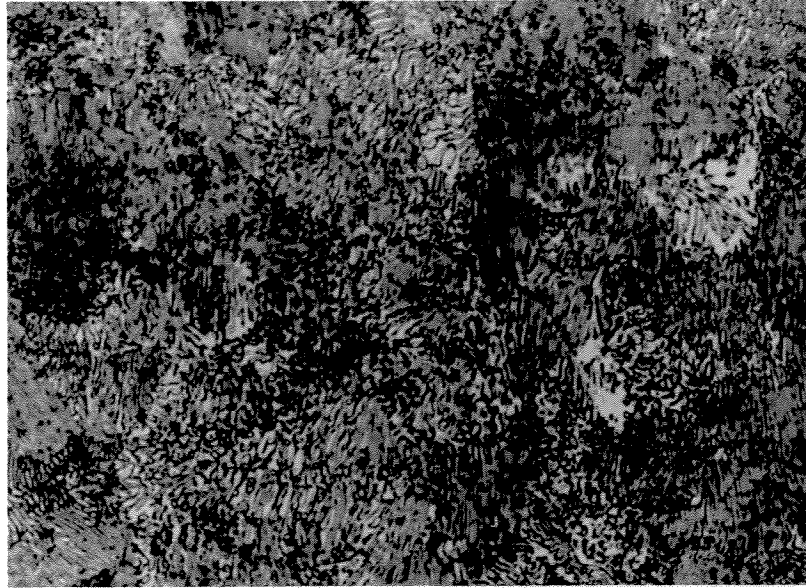


Figure 5.2: Microstructure of the eutectoid steel after being homogenised to minimise the compositional variation. Mag. x800

5.2 Isothermal and Cooling Apparatus

The isothermal and continuous cooling transformation measurements were made using the Gleeble 1500 Thermal-Mechanical Simulator. The tubular specimens, 20 *mm* in length with an 8 *mm* outer diameter and a 1 *mm* wall thickness, were held in place by a tubular stainless steel support assembly, as shown in Figure 5.3.

The severity of the thermal gradient that might arise through the wall thickness of the tubular specimen was analysed on the basis of the Biot Modulus, which is a measure of the internal resistance relative to the external resistance to heat flow for heating or cooling of the specimen. A Biot number of 0.032 was determined which indicates that the thermal gradient across the thickness of the specimen is expected to be insignificant. The details of this analysis are included in Appendix A.1.

The temperature of the specimen was controlled and monitored using an intrinsic Chromel-Alumel thermocouple which was spot welded onto the outer surface of the specimen at mid-length. The sample temperature was controlled by resistive heating. Electrical contact between the specimen and the sample holder was obtained initially by manually applying a small amount of compressive force by reducing the jaw spacing. Subsequent contact during the test cycle was maintained with the aid of a constant pressure air ram.

The resistive heating design, together with the temperature feed-back control system of the Gleeble machine, provided rapid response for precise control of specimen temperature during the heating, isothermal holding and cooling cycles of each test schedule.

The diametral dilation of the specimen due to temperature changes or associated with volume changes due to phase transformation was monitored by a *Linear Variable Differential Transformer* (LVDT) C-strain device designed for the Gleeble. However, the original dilatometer design required modification to the two sample-supporting quartz rods to minimise the contact area. This was necessary to assure a uniform temperature field in the cross sectional plane of the specimen during isothermal and cooling tests. Discussions pertaining this effect are included in Appendix A.2. The dilational changes were monitored in the middle of the specimen to eliminate errors arising from axial temperature gradients. Both the dilation and temperature measurements were monitored in the same cross sectional plane and acquired continuously with a common time base in the 8 channel data acquisition system of the Gleeble.

To minimise oxidation during experimentation, the test chamber was evacuated to a pressure less than 3 *mTorr*, then back filled with high purity Argon gas. This procedure was repeated before each test commenced.

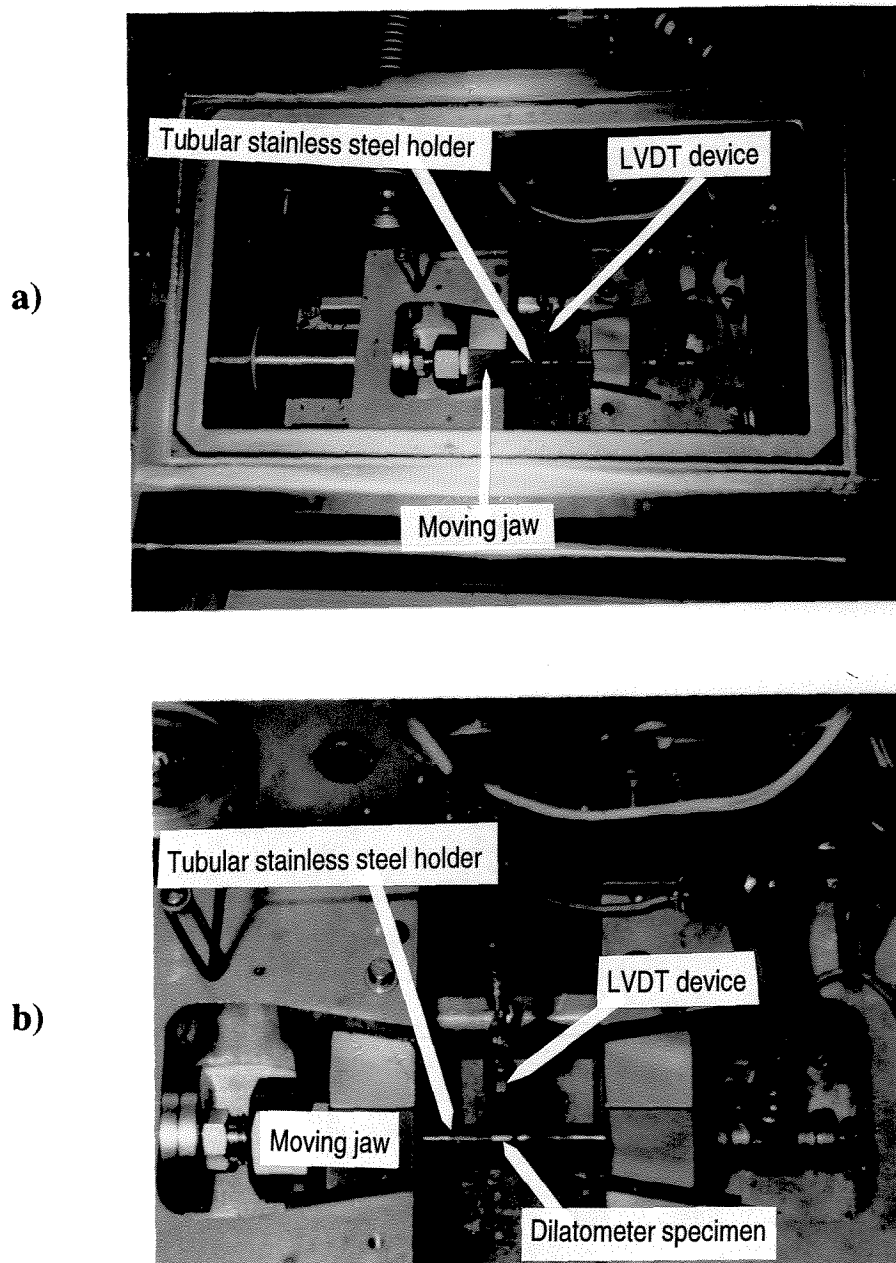


Figure 5.3: The testing chamber of the Gleeble 1500:
a) Overview of the test chamber,
b) Enlargement showing dilatometer specimen, specimen holder and LVDT C-Strain device assembly.

5.3 Isothermal and Cooling Test Procedures

5.3.1 Cooling Schedules

All tests conducted in this study were performed under a high purity argon environment; the chamber pressure was maintained at a pressure that is negative with respect to the ambient to maintain a cover seal, to restrict the in-flow of air that could lead to the oxidation of the sample. Each specimen was first austenitised at 900 °C for 2 minutes, then air cooled to 780 °C, where it was held isothermally for 1 minute before being cooled according to the desired schedule. The isothermal holding of the specimen at an intermediate temperature was carried out in each test to enable the temperature field through the thickness of the specimen to equilibrate. The temperature 780 °C (12 °C above the calculated A_{Cm} temperature) was chosen to avoid any possible nucleation of proeutectoid cementite from austenite.

The cooling schedules employed in this study have been designed to test the additivity concept as it applies to fractional consumption of incubation time, and to provide the data for calculating an ideal *TTT* curve, as derived in Chapter 4. The experimental program encompassed four main cooling regimes:

i) Controlled Cooling Schedule:

To simplify the application of equation (4.17) to derive the ideal incubation time (transformation start time) from a set of continuous cooling data, requires that the data be generated under constant cooling conditions.

Several controlled cooling rates; 0.1, 1.0, 3.0, 7.0 and 10 °C/s, were used in this study to cool each specimen from the austenite phase field to room temperature. The 10 °C/s defines an upper limit for the control cooling by control of the resistive heating current. This range of cooling rates also encompasses those experienced on a Stelmor controlled cooling line.

ii) Isothermal Cooling Schedule:

Conventional isothermal experiments were also carried out to determine the transformation start time at several temperatures from 650 to 680 °C for comparison with the derived ideal transformation start time. The data will also be used to test the predictive capability of an ideal *TTT* curve versus the standard (experimental) *TTT* curve to calculate the Scheil-based continuous cooling start time.

Attempts were also made to conduct tests at temperatures of 640 °C and below. However, at 640 °C the more rapid release of latent heat associated with the faster formation of pearlite, created difficulty in controlling the desired specimen isothermal temperature.

iii) Controlled Isothermal Schedule:

In this schedule, specimens were control cooled at different cooling rates, from 780 °C to 680 °C where they were held isothermally and allowed to transform, and the times to initiate the pearlite formation for each cooling rate was measured.

Data obtained from these tests will be used to deduce the ideal incubation time at 680 °C according to equation (4.13), and will be compared against the ideal *TTT* curve at 680 °C.

iv) Isothermal Step Cooling:

Isothermal step cooling experiments were conducted to assess the capability of Scheil's additivity rule to predict the onset of pearlite formation under non-continuous cooling conditions, based on,

- a) the derived ideal *TTT* curve
- b) the measured conventional *TTT* diagram.

In these tests, specimens having identical solution treatment history were initially cooled to 680 °C and held for a set amount of pre-transformation time (incubation), then rapidly cooled to 670 °C and allowed to transform to pearlite.

Schematic diagrams of the thermal cycles used for the controlled cooling, conventional and modified isothermal and isothermal step cooling experiments are shown in Figure 5.4

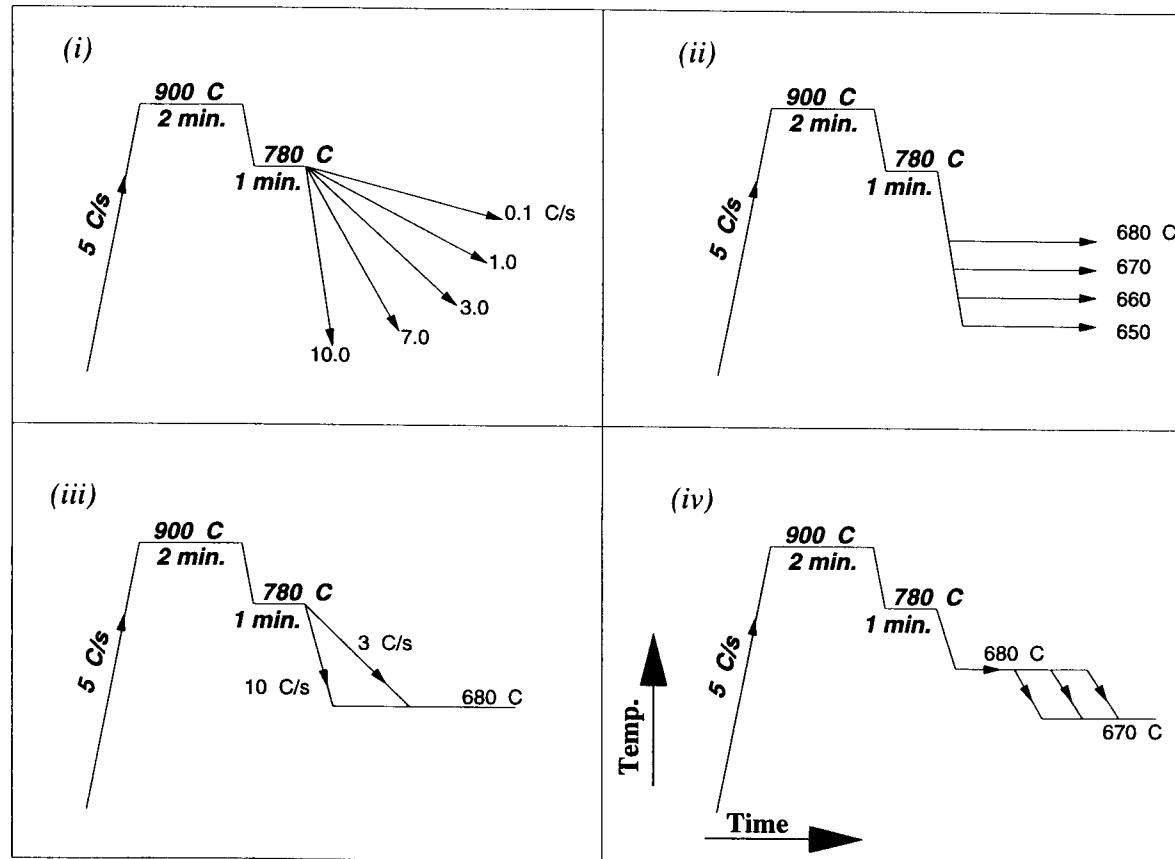


Figure 5.4: Schematic diagram showing cooling schedules for:
i) controlled cooling,
ii) conventional isothermal,
iii) controlled isothermal and,
iv) stepped isothermal tests.

5.3.2 Analysis of Experimental Data

Throughout the analysis of the Gleeble dilatometric data, the measured contraction of the austenite phase due to decreasing temperature was assumed to vary linearly with temperature,^[85] and the onset of the transformation from austenite to pearlite was defined as the point at which the dilation began to deviate from linearity. It should be noted that the austenitic linear contraction was taken as that measured just above the transformation temperature of 730 °C which minimises the effect of any non-linearity of the thermal contraction.

A regression analysis was used to characterise the pre-transformation contraction of the austenite phase. The deviation of measured data from the linearity was taken as the start of transformation, and was determined by the statistical control method.^[86] The scatter of data about the regression was assumed to be normally distributed until the transformation begins where the scatter (deviation) exceeds three standard deviations. The details of this statistical analysis are included in Appendix A.3.

Chapter 6

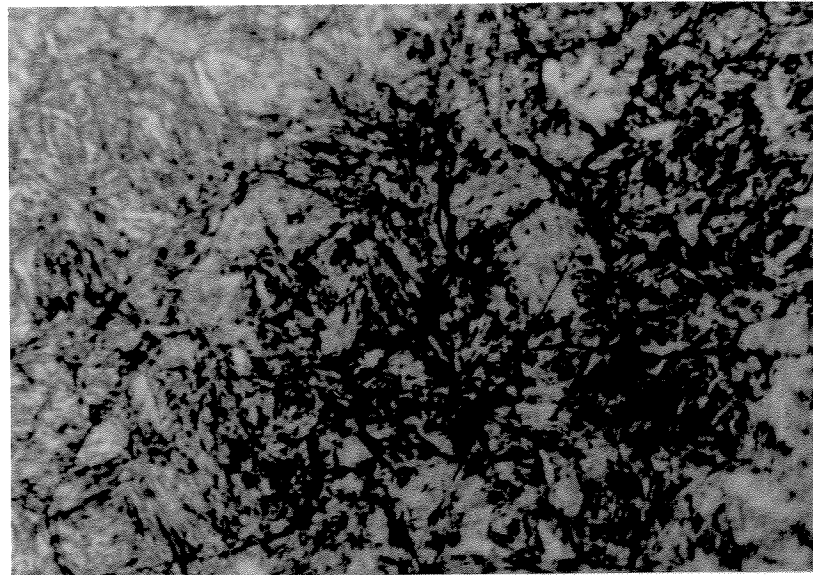
RESULTS AND DISCUSSIONS

6.1 Initial and Final Microstructures

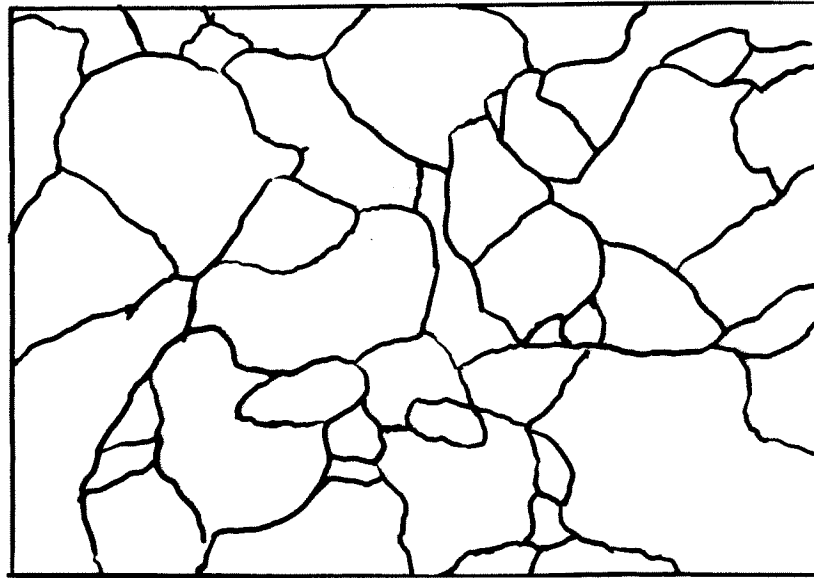
Figure 6.1 is an optical micrograph of a specimen austenitised at 900 °C for 2 minutes, air cooled to 780 °C where it was held for 1 minute to allow the temperature gradient through the wall to equalise then water quenched. The microstructure is predominantly martensite (Figure 6.1 (a)), and shows the grain boundaries of the prior austenite grains, as outlined in Figure 6.1 (b).

A linear intercept method^[89] was used to estimate the mean austenite grain size. Measurements were made over 50 fields of view yielding a mean grain size of 13 μm . This initial microstructure closely reassembles that which exists in steel rod as it exits from the last rolling stand; the mean austenite grain diameter has been reported to be in the range of 10 to 20 μm .^[4,90-92]

The final microstructures resulting from various cooling schedules are shown in Figures 6.2 to 6.4. Figure 6.2 shows the pearlitic structure in a specimen that was control cooled at 3 °C/s to 680 °C, where it was then held isothermally. The resulting microstructure of a specimen that has undergone the conventional rapid cooling ($\cong 100$ °C/s) to the isothermal temperature of 650 °C is shown in Figure 6.3. Finally, the microstructure of an air cooled specimen, which incurred a cooling rate of 14 °C/s at A_{e1} and the transformation initiated at 621 °C during cooling, is shown in Figure 6.4.



(a)



(b)

Figure 6.1: Microstructure of the austenitised, quenched specimen etched in alkaline sodium picrate to reveal the prior austenite grain boundaries. (a) optical micrograph at a magnification $\times 1000$, (b) outline of the grain boundaries.

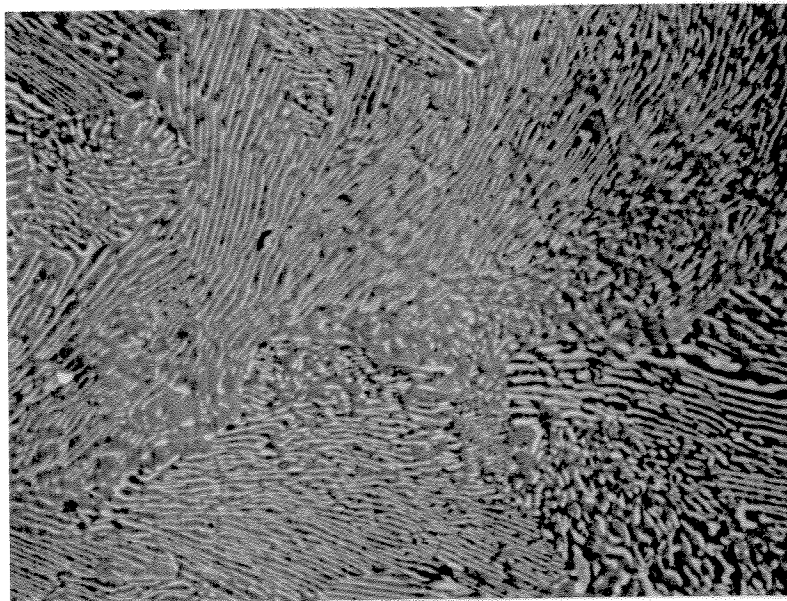


Figure 6.2: SEM microstructure of a specimen control cooled at 3 °C/s to 680 °C, isothermally transformed to pearlite and air cooled to room temperature. Magnification x2000.

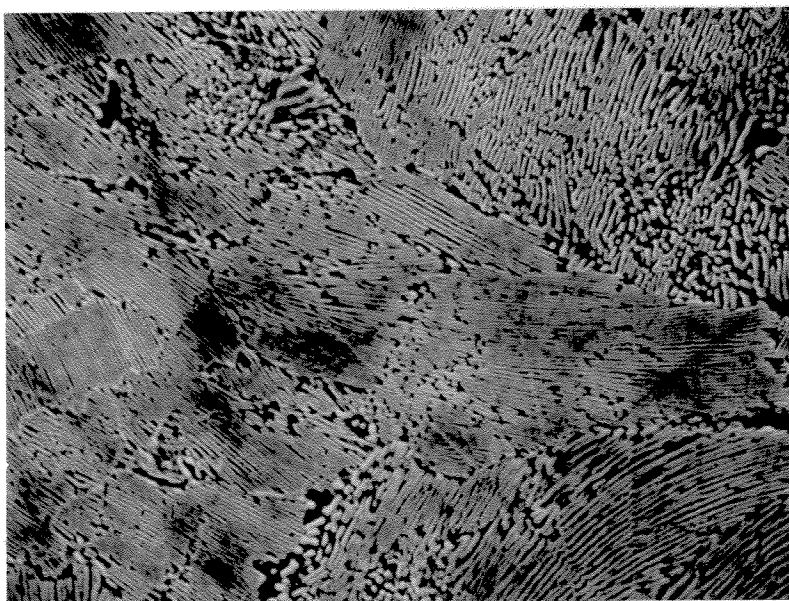


Figure 6.3: SEM microstructure of a specimen rapidly cooled to 650 °C, isothermally transformed to pearlite and air cooled to room temperature. Magnification x3000.

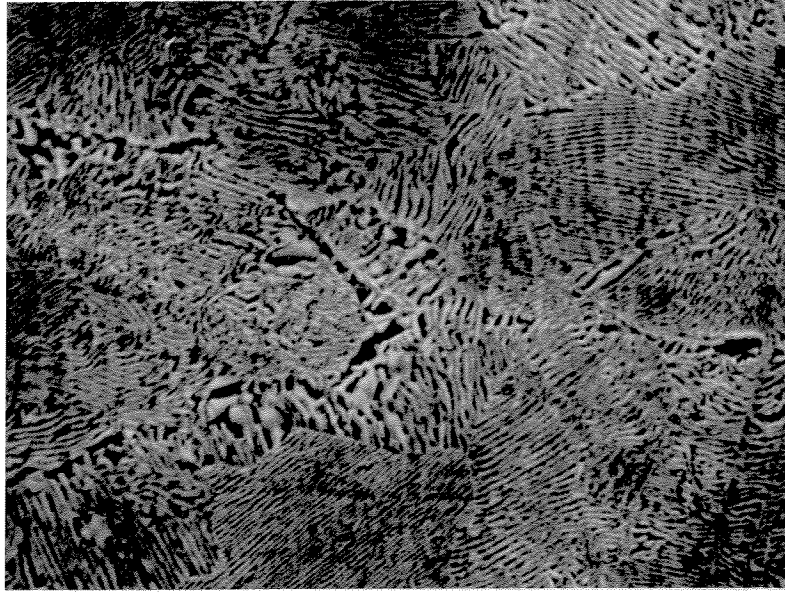


Figure 6.4: SEM microstructure of a specimen air cooled to room temperature by natural convection and radiation, showing primarily pearlite structure. Magnification x4000.

6.2 The "Ideal" Incubation Time

6.2.1 Application of Inverse Additivity

The start of the pearlite transformation, observed under constant cooling rate conditions, is shown in Figure 6.5. The cooling time is the time below the equilibrium austenite decomposition temperature, Ae_1 . The line of best fit obtained from the interpolation is also included in this figure.

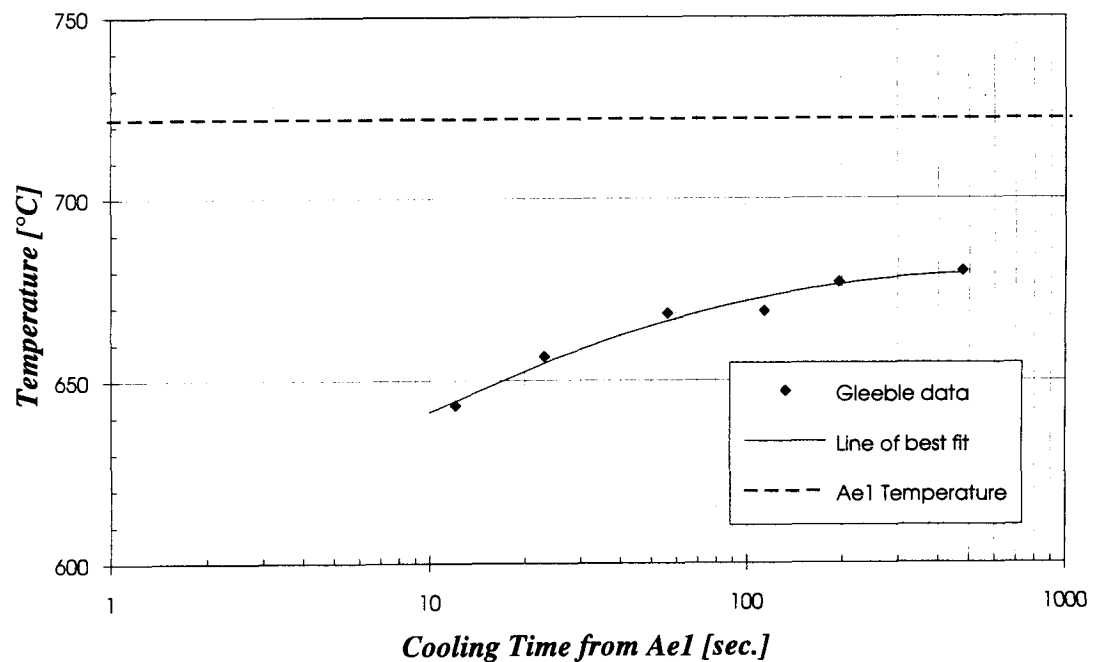


Figure 6.5: Continuous cooling transformation diagram for eutectoid steel under constant cooling rate conditions.

The interpolation thus represents the locus of the start of the transformation to pearlite under constant cooling rate conditions. Accordingly, from this figure, the cooling rate to attain a given amount of undercooling before the onset of pearlite formation can be determined as follows:

$$\dot{\theta}_c = \frac{\Delta T_{CCT}}{t_{CCT}} \quad \dots(6.1)$$

where ΔT_{CCT} and t_{CCT} are the amount of undercooling and cooling time from the Ae_1 to the start of the pearlite transformation, respectively.

Making use of equation (6.1) and the best fit to the experimental constant cooling rate data, a curve of the limiting cooling rate as a function of the degree of undercooling is shown in Figure 6.6. The resulting limiting cooling rate curve in Figure 6.6 represents the slowest cooling rate required to reach a given amount of undercooling without initiating the transformation to pearlite during cooling.

According to equation (4.17), the "ideal" incubation time, τ , can be found by taking the reciprocal of the gradient of the limiting cooling rate curve with respect to undercooling. The calculation of the "ideal" incubation time, according to inverse additivity, was performed within the experimental range. The results are shown in Figure 6.7 where the "ideal" incubation time was plotted as a function of undercooling.

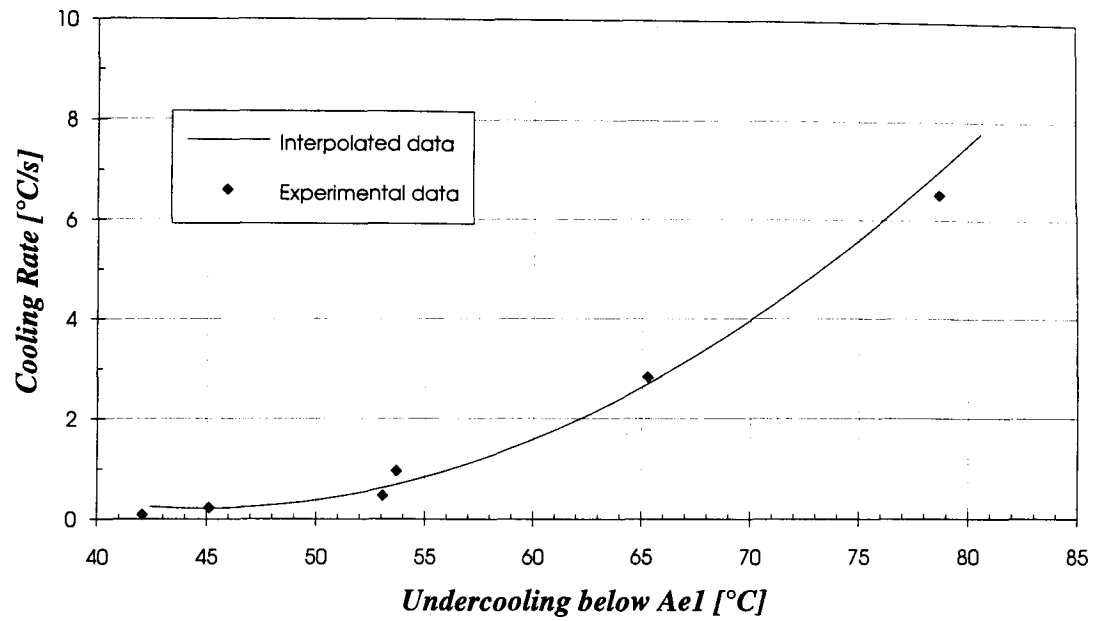


Figure 6.6: Constant cooling rate to reach a given undercooling prior to transformation.

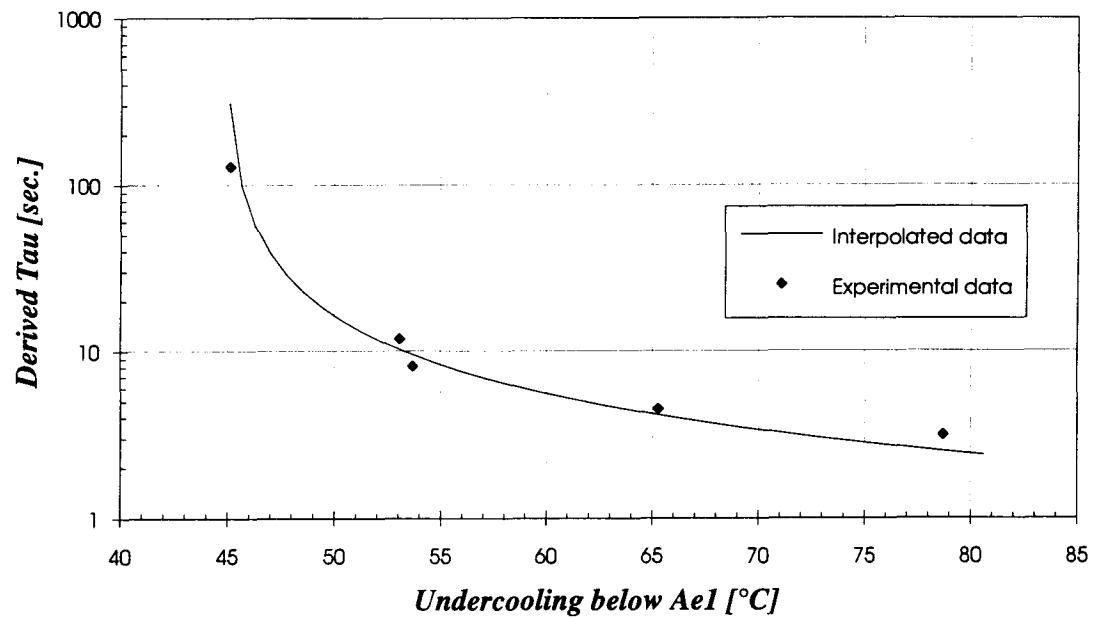


Figure 6.7: The "ideal" incubation time as a function of undercooling.

6.2.2 Expression of The Ideal Incubation Time

The derived "ideal" incubation time, based on the data interpolated within the experimental range, form the basis for the regression of τ as a function of temperature.

In this study, the growth equation (equation (2.19)) has been assumed to adequately describes the relationship between the isothermal transformation start time, τ , and temperature. Although the underlying assumption of this type of equation is that the site saturation condition prevails in the reaction, a condition which is difficult to assess, its success in describing the "C" curve behaviour of the *TTT* start time for a number of plain carbon steels has been demonstrated by Kirkaldy *et. al.*^[76,78,79]

Linearisation of equation (2.19) yields:

$$\log\left\{\frac{\tau}{\exp(Q/RT)}\right\} = -m \log\{\Delta T\} + \log(A) \quad \dots(6.2)$$

In this analysis, the values of both Q and m were simultaneously determined by varying the value of Q until a best fit of $\log(\tau \cdot \exp(-Q/RT))$ vs. $\log(\Delta T)$ was obtained. The condition of best fit was obtained (correlation coefficient, $r=0.9960$), when the value of Q was 125.6 kJ/mol (30 kCal/mol), the exponent m was 4.15 and the corresponding proportionality constant, A , was 32.5. Figure 6.8 shows the results of the regression analysis in which the triangular points represent the data (as measured and interpolated) within the experimental range, and the line of best fit is shown as a solid line.

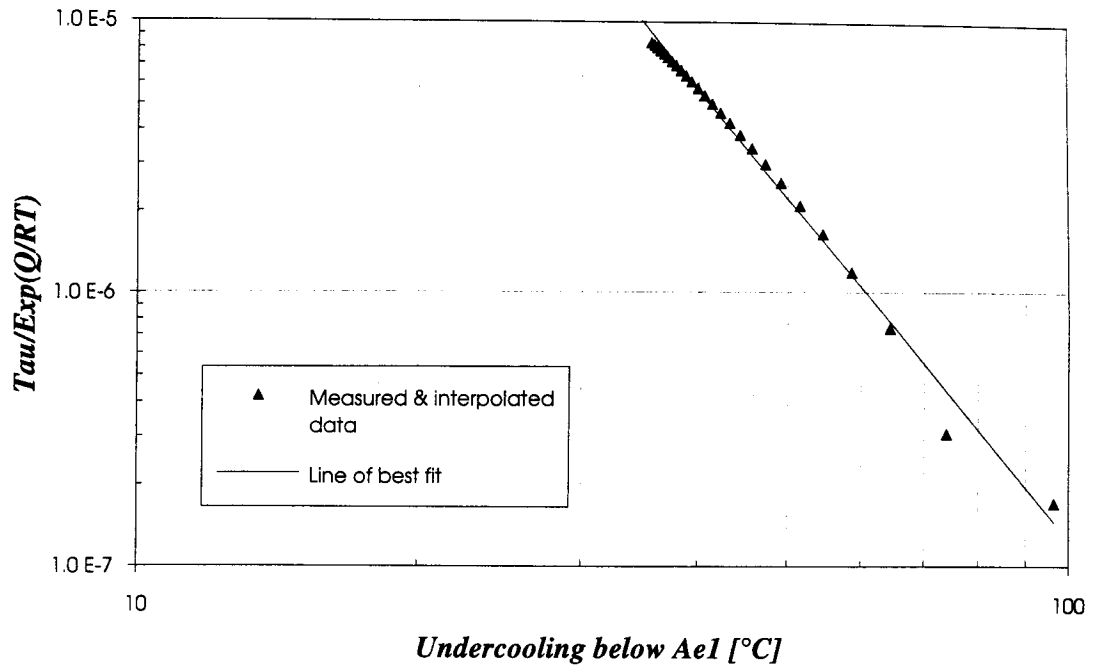


Figure 6.8: Logarithmic plot of the product of incubation time and $\exp(-Q/RT)$ as a function of undercooling below Ae_1 .

Thus, an equation describing the ideal isothermal start transformation time to pearlite for the steel used in this study was found to be:

$$\tau(T) = 32.5 \frac{\exp\left(\frac{125.6 \text{ kJ/mol}}{RT}\right)}{(\Delta T)^{4.15}} \quad \dots(6.3)$$

Figure 6.9 shows the graphical form of equation (6.3) in the temperature-log(time) plot. Included in this figure are the transformation start results obtained from the conventional isothermal experiments. As anticipated from the preceding discussions in

Chapter 4, since there is a finite amount of fractional incubation time consumed during the initial cooling of the specimen to the desired isothermal temperature in the conventional *TTT* test, the observed start for these tests were expected to be delayed relative to the "ideal" *TTT* curve.

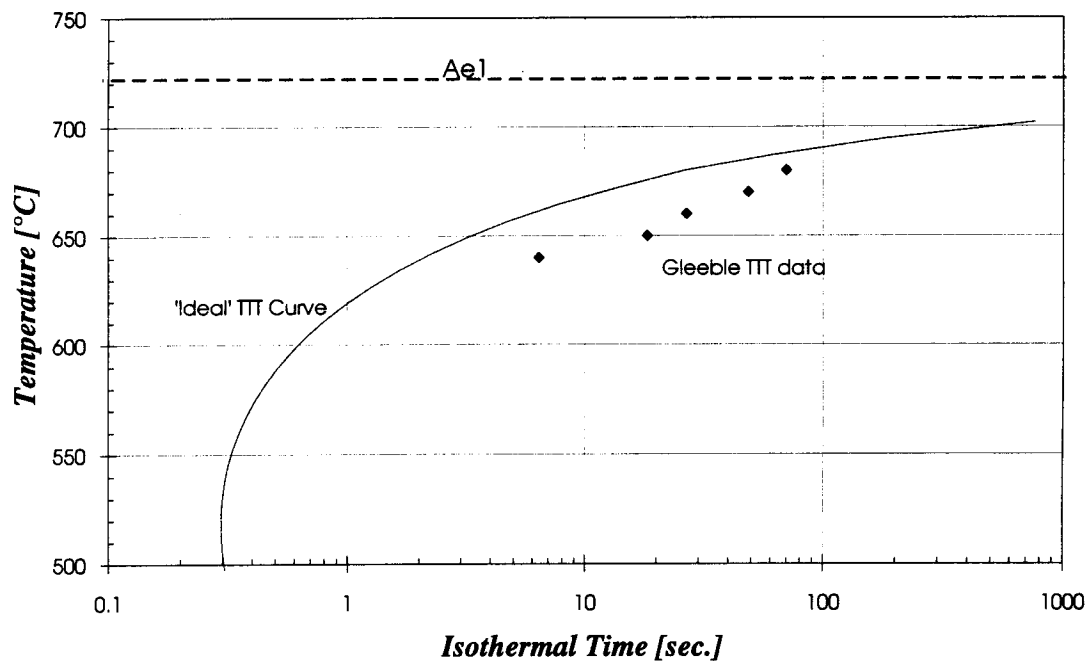


Figure 6.9: The "ideal" isothermal transformation (*TTT*) diagram.

The results of the regression suggest that the activation enthalpy for the diffusion of carbon in austenite, associated with pearlite formation, is 125.6 kJ/mol (30 kCal/mol). This value is similar to that estimated by Zener,^[61] who reported a value of 150 kJ/mol (36 kCal/mol) as the activation energy for diffusion of carbon during pearlite growth.

As suggested by Kirkaldy *et. al.*,^[76] the proportionality constant, A , contains the grain size and composition dependent parameters. However, analysis of A in terms of the constituents was not possible in this study, since only one steel grade was used and the austenitising condition was chosen to yield a similar microstructure to that present at the exit of the last rolling stand.

The supercooling exponent m , typically signifies the predominant mode of diffusion responsible for the reaction; physical meaning is associated with a value of 2 or 3. However, the exponent of 4.15 obtained in this study is an empirical constant that resulted from maximising the regression coefficient to ensure the best fit with the experimental data.

Comparison of the derived "ideal" TTT curve to a curve that is predicted according to Kirkaldy and Venugopalan^[79] for 0.1% transformed, for the steel composition shown in Table 5.1 and an initial austenite grain size of $13\ \mu m$ (ASTM grain size number 9) is shown in Figure 6.10. The transformation time to 0.1% pearlite was calculated according to the formulae given by Kirkaldy and Venugopalan^[79] as follows:

$$\tau_{0.1\%} = \frac{1.79 + 5.42(Cr + Mo + Mo \cdot Ni)}{2^{\frac{(G-1)}{2}} (\Delta T)^3 D} \int_0^{0.1\%} \frac{dx}{x^{\frac{2}{3}}(1-x)^{\frac{2}{3}}} \quad \dots(6.4)$$

where G is the ASTM grain size number and D is the diffusion coefficient which is evaluated as follows:

$$\frac{1}{D} = \frac{1}{\exp\left(\frac{-27.5kCal/mol}{RT}\right)} + \frac{0.01Cr + 0.52Mo}{\exp\left(\frac{-37kCal/mol}{RT}\right)} \quad \dots(6.5)$$

Figure 6.10 shows that equation (6.4) predicts a 0.1% transformation line that is almost a decade to right of the "ideal" *TTT* at the nose temperature. At higher temperatures, approaching the A_{e1} , Kirkaldy's predicted curve lies at shorter times.

It should be noted that the ideal *TTT* curve was derived from experimental dilatometry in which the deviation from linearity in the dilation-temperature relationship was taken as the start of transformation. Specimen quenched at this condition and examined metallographically did not reveal any pearlite under the resolution of the optical microscope. Specimens quenched after this dilation transition did show increasing amounts of pearlite. Consequently, the dilation transition is consistent with the initial stage of decomposition, and therefore, would be expected to compared with the 0.1% transformation line. There is insufficient evidence to provide any plausible explanation on the cross-over of the two curves at above 670 °C, although it is acknowledged that Kirkaldy's equation represents an average for a wide range of compositions and grain sizes.

While there is no published isothermal transformation diagram for the specific steel chemistry used in this study, comparison of the characteristic features of the derived ideal *TTT* curve to those of a standard *TTT* curve reported for a 1080 steel in the *Atlas of Isothermal diagrams* is shown in Figure 6.11. This 1080 steel^[29] contained 0.79 wt%C, 0.76 wt%Mn, and was austenitised at 900 °C (1650 °F) to give an ASTM grain size of 6.

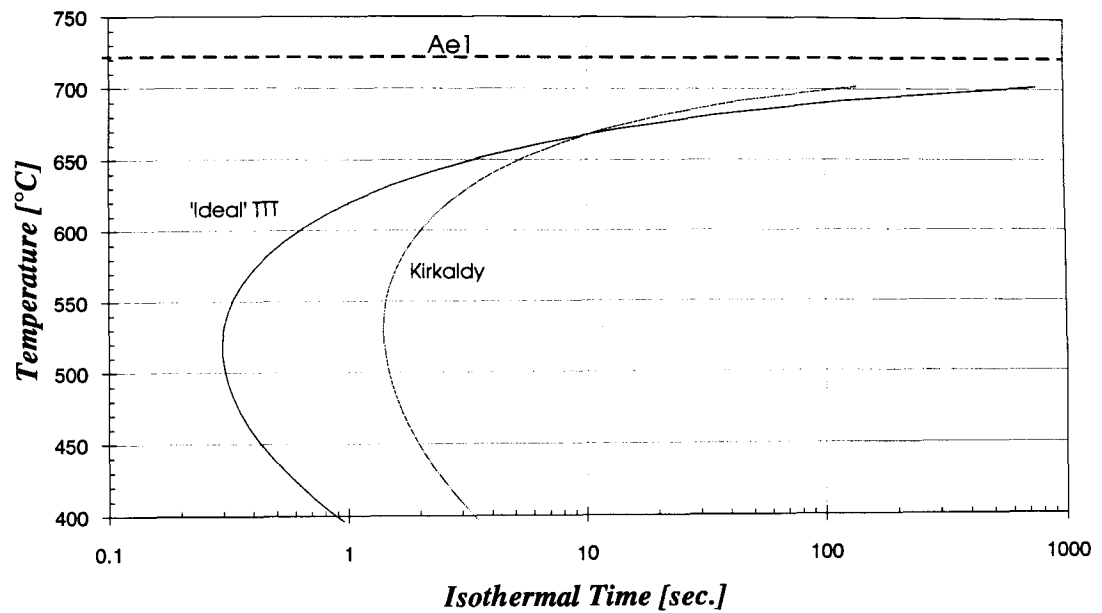


Figure 6.10: Comparison of the derived ideal *TTT* curve to the curve for 0.1% transformation by Kirkaldy & Venugopalan.^[79]

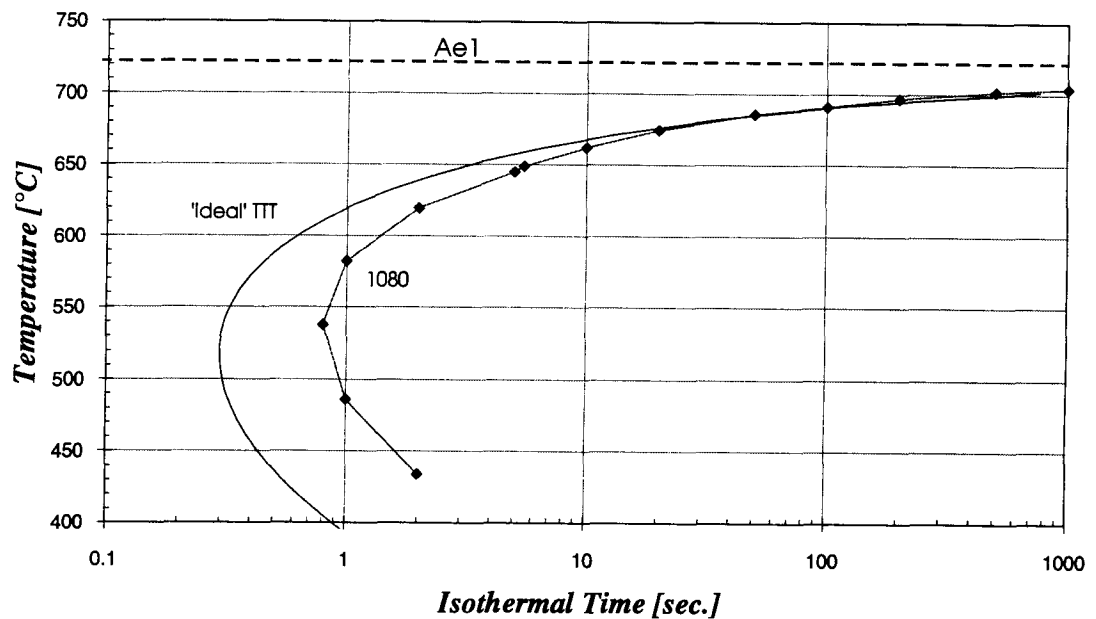


Figure 6.11: Comparison of the derived ideal *TTT* curve with the published literature for a 1080 *TTT* curve.^[29]

It can be seen from Figure 6.11 that the shape of the two curves are very similar with the ideal *TTT* curve lying to the left (shorter time) of that of the published curve for the 1080 steel. The "nose" temperature of the 1080 steel *TTT* curve was suggested to be approximately 535 °C and the corresponding time of 0.8 seconds, while the ideal *TTT* curve shows a "nose" temperature of approximately 520 °C and a minimum isothermal time of 0.3 second. At high temperatures, the two curves converge into one.

The consistency of deducing the "ideal" incubation time by means of the additivity rule, both in the forward and in the inverse application, was also examined in this study.

Controlled isothermal experiments were conducted in which specimens were controlled cooled at different rates from 780 °C to 680 °C, where they were then held isothermally. The experimental time to reach the isothermal temperature, and the time to detect the formation of pearlite, were measured and tabulated in Table 6.1.

Table 6.1: Experimental times obtained from the controlled isothermal experiments.

Cooling Conditions	Experimentation Time in seconds to:		
	780 °C	680 °C	Start
3 °C/s->680 °C	0.00	33.08	66.44
10 °C/s -> 680°C	0.00	10.04	54.11

From the discussion in Section 4.1.1, the "ideal" incubation time can be deduced directly according to equation (4.13) as follows:

$$\tau_T = \frac{\dot{\theta}_{C1}t_{s1} - \dot{\theta}_{C2}t_{s2}}{\dot{\theta}_{C1} - \dot{\theta}_{C2}} \quad \dots(6.6)$$

where θ_{Ci} and t_{si} are the rate of controlled cooling and the experimental time for the start of transformation at temperature T , respectively. Using the results in Table 6.1, the ideal incubation time at 680 °C is thus:

$$\begin{aligned} \tau_{680^\circ C} &= \frac{10 \times 54.11 - 3 \times 66.44}{10 - 3} \\ &= 48.82 \quad [\text{sec.}] \end{aligned}$$

while evaluation of τ at 680 °C, according to equation (6.3), yields 45.16 seconds. The incubation time at 680 °C derived by the two different methods may be deemed to be in good agreement.

6.3 Predicting The Start of Transformation to Pearlite

6.3.1 Based on The "Ideal" Incubation Time

A test of Scheil's additivity rule, based on the derived "ideal" incubation time function, to predict the start of transformation to pearlite was carried out using three different cooling patterns. Figure 6.12 shows the thermal histories of two Newtonian cooling conditions employed in this study. In one case, a specimen was allowed to cool naturally by radiation and free convection inside the test chamber; while in the other case, the tubular specimen was forced cooled by the flow of helium gas along its internal diameter. In both cases, the diametral dilation and specimen temperature were continuously recorded with the same time base. The average cooling rates at the A_{e1} were measured to be 14 °C/s for natural cooling and 42 °C/s for the helium quench condition. These two cooling situations thus represent the typical, and an exaggerated continuous cooling processes that could be encountered in industrial cooling.

A simulation of rod cooling on the Stelmor conveyor was also conducted on the Gleeble based on the temperature measurements obtained^a at the Rod Mill of BHP Rod and Bar Product Division in Newcastle, Australia. Figure 6.13 shows the mill data (square points)

a Data were compiled and made available by Mr. Ron Gloss of BHP Research, Melbourne Laboratories.

and the Gleeble simulation of the rod cooling from the laying head where its temperature was 880 °C. Once again, the diametral dilation was simultaneously recorded with the specimen temperature during the simulation.

Making use of the derived "ideal" incubation time function, $\tau(T)$, equation (6.3), and Scheil's additivity rule,

$$\int_{T=AeI}^{T=ArI} \frac{dt}{\tau(T)} = 1 \quad \dots(6.7)$$

the start of pearlite transformation was determined based on the thermal history for the three previously described different cooling conditions. The observed transformation start times, which were determined based on the dilation-temperature information, according to the method described in Section 5.3.2, were used as a means of testing the proposed procedure.

The results of the predicted and measured start of transformation of austenite-to-pearlite under the two Newtonian and the Stelmor simulation are shown in Figure 6.14. In this figure, the measured transformation start for the two Newtonian cooling conditions are shown with the diamond symbols; while the solid triangle represents the transformation start measured from the Stelmor simulation. The predicted start of transformation according to Scheil's additivity rule, based on the ideal TTT curve (or the ideal incubation time function), are indicated as squares.

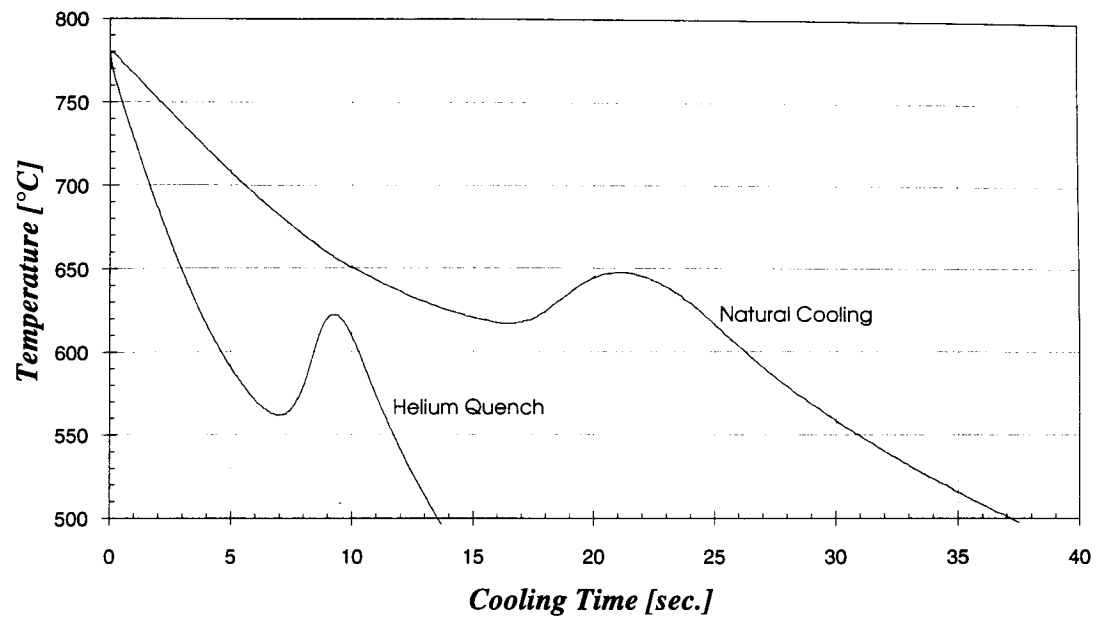


Figure 6.12: Thermal histories of the Newtonian cooling situations used in this study.

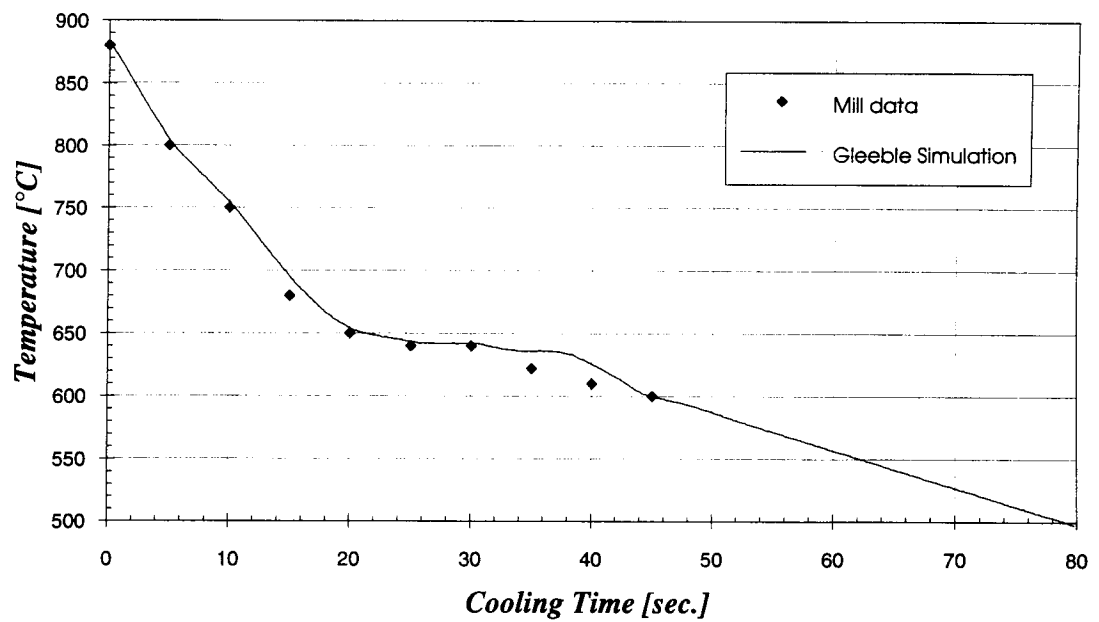


Figure 6.13: Simulation of rod cooling on a Stelmor conveyor.

The predictions of the transformation start for all three cooling conditions slightly preceded the experimental measurements; this is in contrast to previous observations in which the Scheil's additivity rule was found to over predict the transformation start.^[40-42,65,66] However, it should be emphasized that both Newtonian coolings and the Stelmor simulation incurred cooling rates beyond the experimental conditions which were used to derived the "ideal" incubation curve. In this regard, the predictions are deemed to successfully predict the start of transformation for the continuous and "semi-continuous" cooling conditions employed.

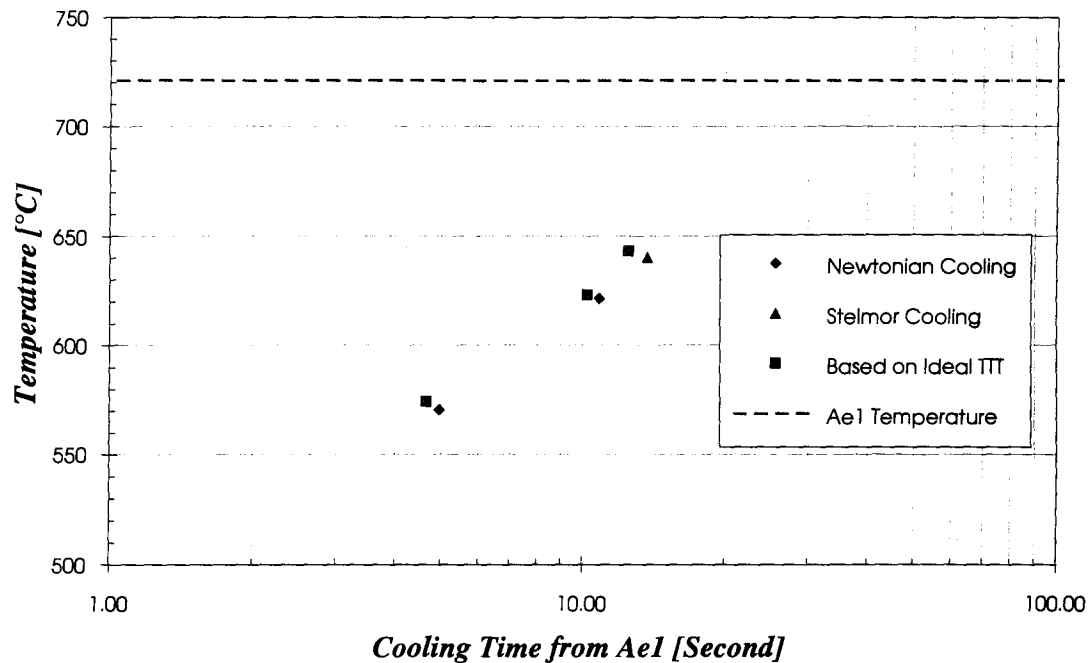


Figure 6.14: Predicted and measured transformation start under Newtonian coolings and Stelmor simulation conditions.

The ability to predict the transformation start under non-continuous cooling conditions was also examined in this study. After being solution treated, specimens were rapidly cooled to 680 °C where they were held isothermally for pre-transformation time of 5, 15 and 30 seconds, respectively, then rapidly cooled to 670 °C and allowed to transform to pearlite (see Figure 5.2(iv)). Other tests which are in fact also non-continuous are the controlled isothermal (Figure 5.2(iii)) and the conventional isothermal or *TTT* tests (Figure 5.2(ii)). Each involves at least one abrupt change in the cooling rate.

The start of transformation to pearlite was predicted based on the ideal *TTT* curve, the Scheil additivity rule and the thermal histories of each test and compared to those obtained from the experimental dilation-temperature information. Figure 6.15 shows a plot of the predicted time, from A_{e_1} , for start of transformation as a function of the measured starting times; the line of ideality is also indicated in this figure.

The results show that the predictions are consistently 10 seconds ahead of the measured values, with a standard deviation of 10.74 seconds. When the results from the Newtonian and Stelmor cooling conditions are also considered, it can be seen that the predictions from this method are very consistent and slightly ahead of the measured data, regardless of the cooling pattern employed. Thus, this method of predicting the transformation start is considered to be reasonably promising.

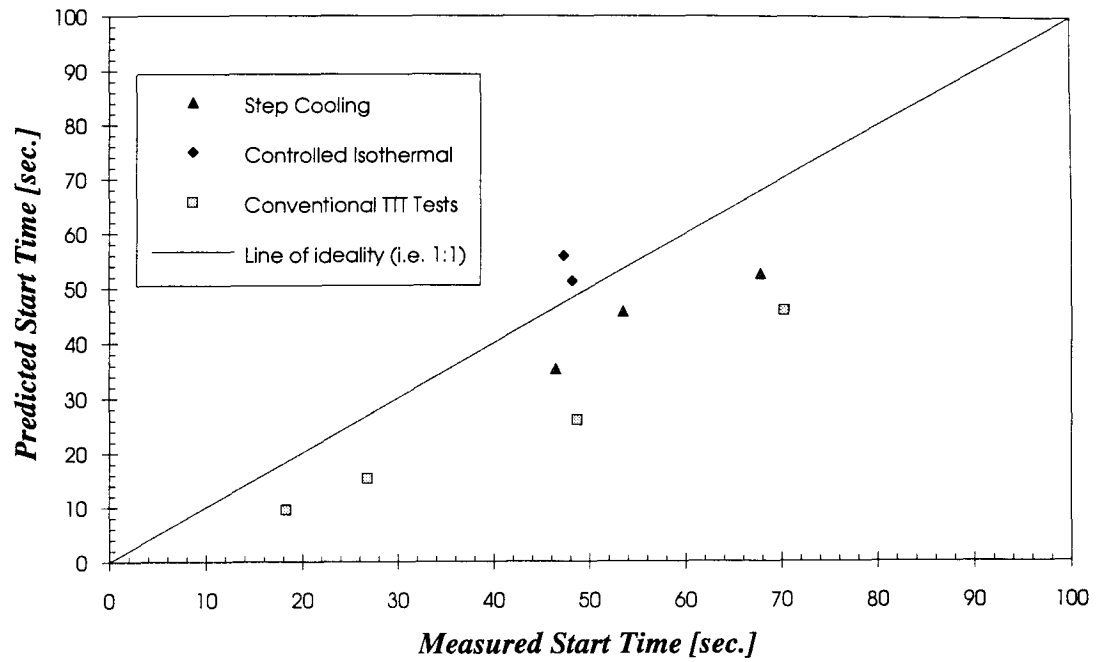


Figure 6.15: Predicted and measured transformation start for non-continuous cooling conditions.

6.3.2 By Conventional Methods

6.3.2.1 Using Cooling Rates at Ae_1

Predictions of the start of transformation to pearlite for the two Newtonian coolings and the Stelmor simulation have also been made based on the cooling rates at Ae_1 , a technique which has been widely used.^[13-15] From the results of constant cooling rate experiments, a regression analysis was carried out to obtain an analytical expression for the transformation start temperature, T_s , as a function of cooling rates. The best correlation was found when T_s was plotted against the logarithmic of the cooling rates, this is shown in Figure 6.16. An equation expressing T_s , in °C, as a function of the cooling rates was found to be:

$$T_s = 663.82 - 19.3 \log(\dot{\theta}) \quad \dots(6.8)$$

with the coefficient of determination, r^2 , being 0.9404.

The average cooling rates at Ae_1 of the two Newtonian coolings and the Stelmor simulation were measured from the thermal history data, and the transformation start temperatures were estimated using equation (6.8). Figure 6.17 shows the comparison between the measured dilation-temperature data, represented by the square data points, and the predictions based on the cooling rates at Ae_1 , shown by the filled triangles.

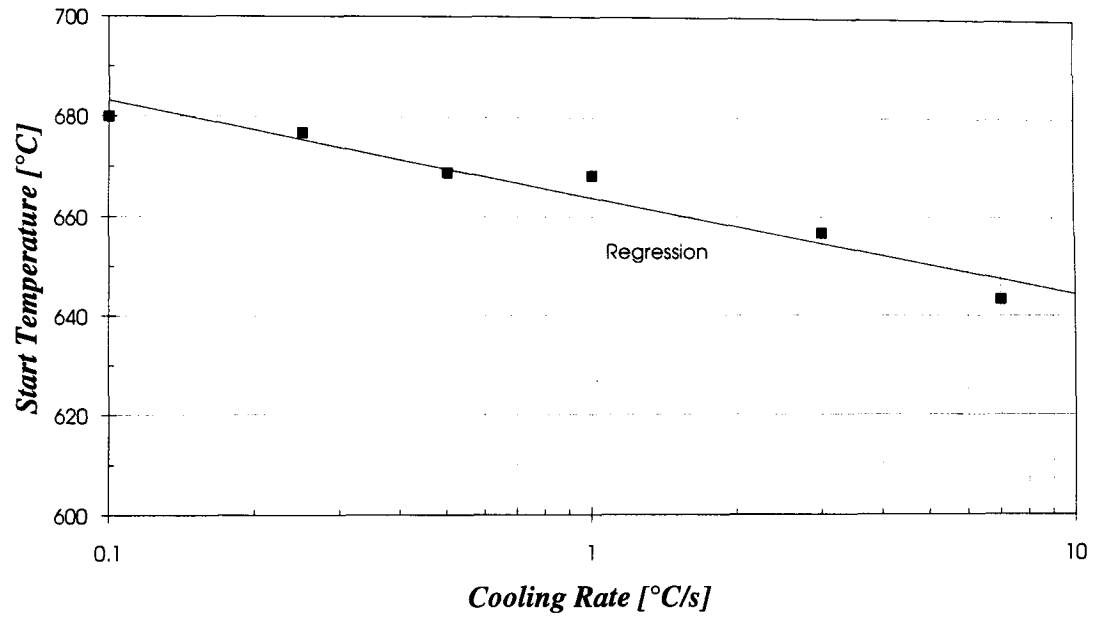


Figure 6.16: Correlation between the transformation start temperature and the cooling rate.

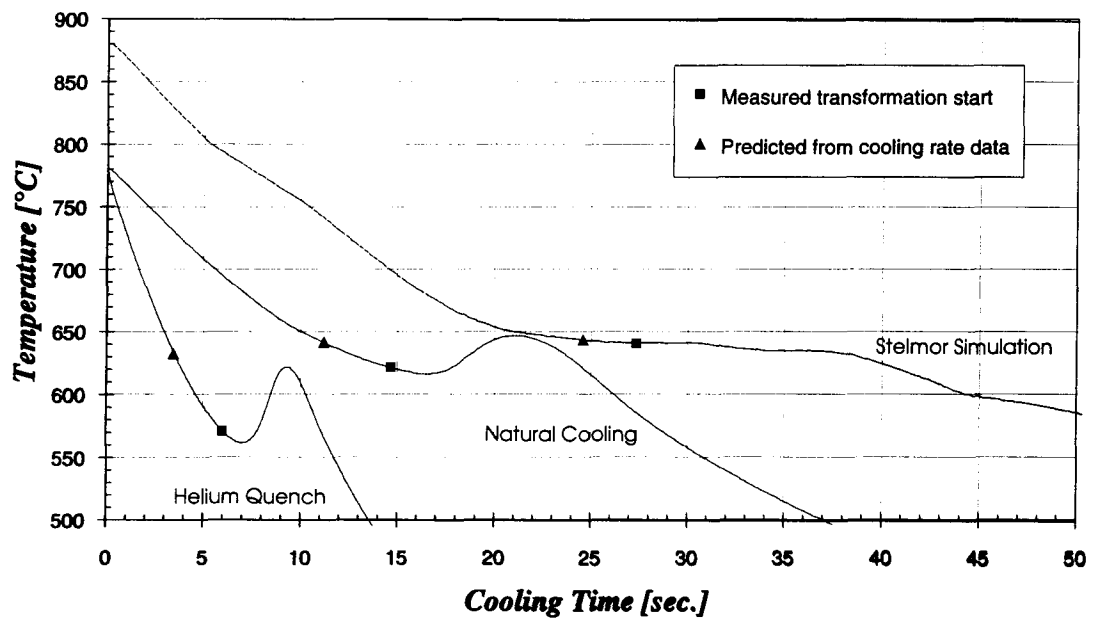


Figure 6.17: Predicted and measured transformation start times under the Newtonian coolings and Stelmor simulation conditions, using cooling rates at the Ae_1 .

For the Stelmor simulation case, the prediction was reasonably close to the experimentally measured values, while for the helium quench condition, the prediction was premature by as much as 60 °C. This increased discrepancy, observed as the cooling rate increases, reflects the empirical nature of this technique.

While this empirical technique of estimating the transformation start temperature has been commonly used, there is no theoretical justification for it, and consequently, it relies on the availability of experimental data to provide the empirical cooling rate-transformation start temperature relationship. The results in Figure 6.17 clearly demonstrate that the relationship can not be projected beyond the experimental range over which the regression was carried out.

6.3.2.2 Based on Experimental TTT Results

It has been reported in a number of studies^[40-42,65] that the experimentally generated *TTT* curves can be used as a basis for applying the Scheil's additivity rule to predict the transformation start. This method of prediction was also examined in this study.

Regression analysis was carried out to describe the isothermal transformation start time as a function of temperature (incubation time) for the experimental *TTT* data. The line of best fit, using the growth equation (equation (2.19)), was found to be as follows:

$$\tau(T) = 498.5 \frac{\exp\left(\frac{125.6 \text{ kJ/mol.}}{RT}\right)}{(\Delta T)^{4.69}} \quad \dots(6.9)$$

The graphical form of this expression is shown in Figure 6.18, along with the experimental data used for the regression. Figure 6.18 also includes the *TTT* curve reported for a 1080 steel^[29] and the derived "ideal" *TTT* curve for comparison.

By comparing the "ideal" *TTT* and the experimental *TTT* curves it can be seen that experimental *TTT* curve lies almost one decade to the right of the "ideal" *TTT* curve at the "nose" temperature. However, the regressed experimental *TTT* curve is quite similar to the curve for a 1080 steel with a constant shift to the right; both curves have a "nose" temperature in the vicinity of 530 °C. At the nose temperature, the regressed experimental *TTT* curve is less than one second to the right of that for 1080 steel.

The Scheil's additivity rule, equation (6.7), was used with equation (6.9) to determine the transformation start for the two Newtonian coolings and the Stelmor simulation. The results are shown in Figure 6.19, in which the predictions are represented by triangles, while the measured results are shown as squares. The predictions of the transformation start for each condition were late in all cases. This is in accordance to the observation reported by Hawbolt *et. al.*^[65]

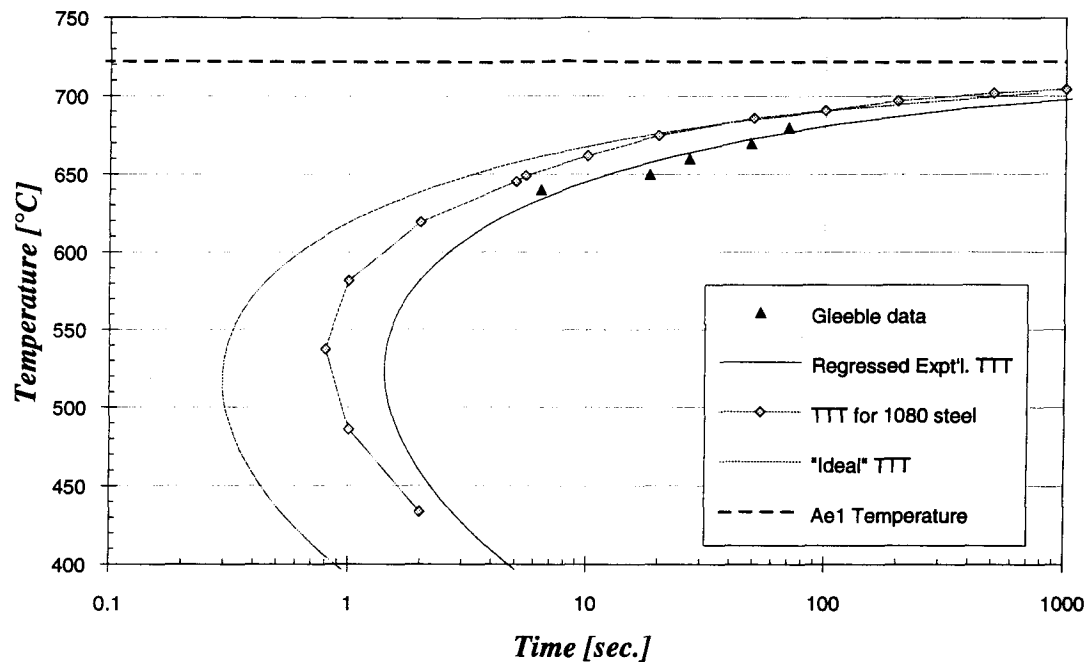


Figure 6.18: The experimental *TTT* curves.

Figure 6.20 shows the predicted results versus the measured start times from Ae_1 when this procedure was applied to the controlled isothermal and step isothermal experiments. While the predictions for the isothermal step tests alone were very good,

the predictions for the cooling rate controlled isothermal tests were far from the measured values; combining these results gives an overall prediction of about 24 seconds late with a standard deviation of 38.8 seconds.

For the three cooling conditions used, the overall prediction of the Scheil's additivity rule, based on the experimental *TTT* curve, is generally late, except for the stepped isothermal tests.

It should be noted that the initial cooling rate in the stepped tests was the same as that incurred in the conventional isothermal tests. This means that the fractional incubation consumption associated with the transient cooling in the two situations is the same. The close agreement between the predicted and measured transformation start in the stepped isothermal tests suggests that the use of Scheil's additivity rule is valid in such circumstances.

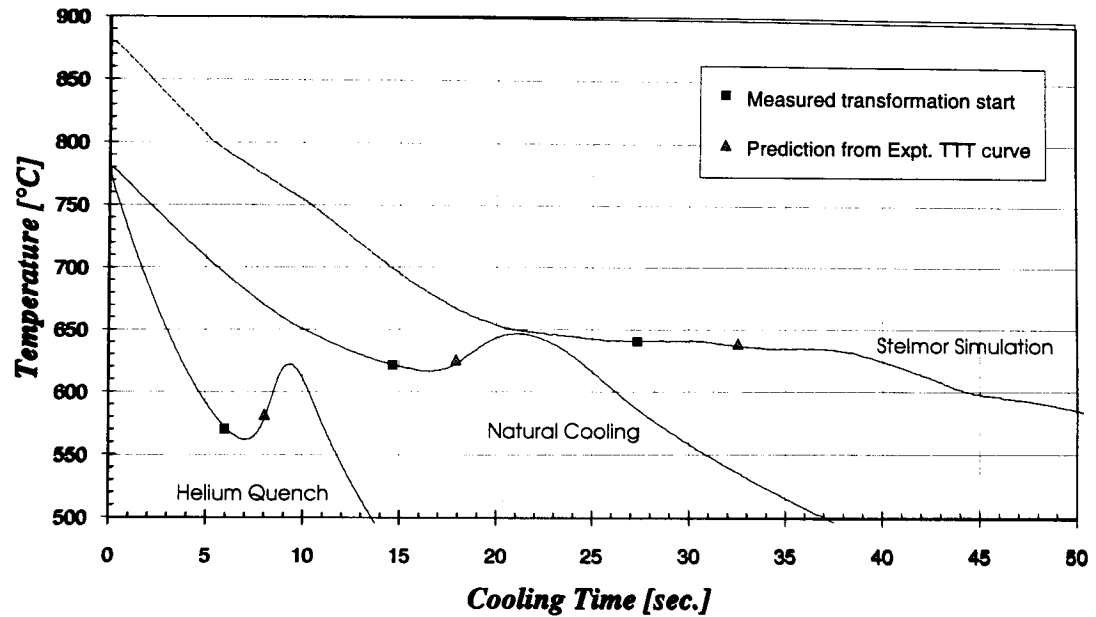


Figure 6.19: Predicted and measured transformation start times for the two Newtonian coolings and the Stelmor condition, based on the experimental *TTT* curve.

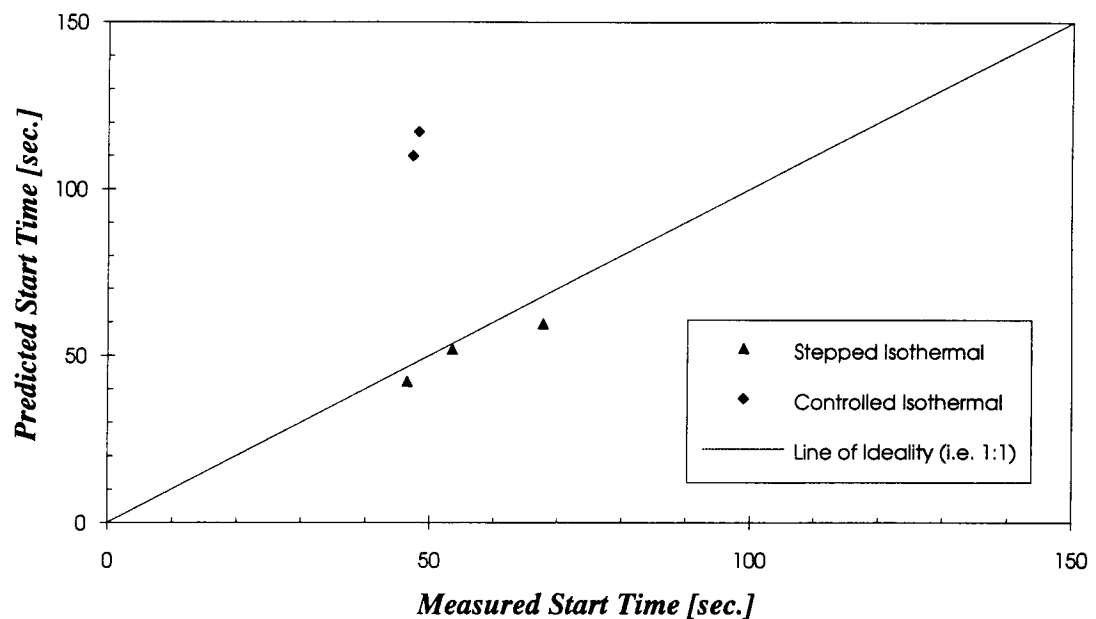


Figure 6.20: Predicted and measured transformation start times under the non-continuous cooling conditions, based on experimental *TTT* curves.

6.3.3 Prediction Capability of the Three Methods

Among the three methods for predicting the start of transformation from austenite to pearlite examined in this study, the predictions based on the cooling rate at A_{e1} only provides the temperature at which transformation start is expected to occur. To completely define the transformation starting condition, the corresponding time must also be obtained from the cooling data. In essence, this method of prediction is insensitive to changes in the thermal condition experienced by the specimen below the temperature range where the cooling rate was determined. Consequently, it is not suitable for application to non-continuous cooling conditions.

For the semi-continuous cooling condition (i.e., the Stelmor cooling simulation) considered in this study, which has a cooling rate of $11.4\text{ }^{\circ}\text{C/s}$ at A_{e1} , the prediction based on cooling rate was in reasonable agreement with the measured transformation start. However, the cooling rate for this cooling condition is very close to that from which equation (6.8) was obtained. Furthermore, it should also be noted that the controlled cooling schedule used at the Stelmor facility has been designed to obtain the transformation within the steel rod at $640\text{ }^{\circ}\text{C}$.

On the other hand, prediction of the transformation start by Scheil's additivity rule takes into account the thermal history of the specimen as it integrates the fractional incubation consumption below the A_{e1} . The choice of the "best" *TTT* curve for this analysis is dependent on the validity of this method in predicting the start of transformation.

Since there is a finite amount of fractional incubation consumed associated with the initial transient cooling during the generation of an experimental *TTT* curve, this effectively displaces the *TTT* curve obtained to longer times. However, when an experimental *TTT* curve is used as the basis for applying the Scheil additivity rule, the inherent fractional incubation consumed is implicitly ignored, resulting in over-estimation of the transformation start, as evidence in this study and others.^[40-42,65,66]

Consistent results have been found with the prediction of the transformation start time based on the ideal *TTT* curve. The prediction has been found to precede the measured start of transformation to pearlite in all cooling conditions employed, which is in contrast to previous reports based on the traditional *TTT* curve.^[40-42,65,66] Excellent agreement between the predicted and measured values was found for the continuous and semi-continuous cooling conditions, while for the non-continuous cooling situation, the prediction compared favourably to the measured results with a mean difference in the start time of 10 seconds, and a standard deviation of 10.74 seconds.

Thus, the performance of the three methods for predicting the start of the pearlite transformation for three very different cooling conditions is summarised as in Table 6.2.

Table 6.2: Comparison of the capability of the three methods in predicting the start of pearlite transformation.

Prediction methods	Cooling conditions		
	Continuous	Semi-Continuous	Non-Continuous
Scheil's rule based on "ideal" TTT^{\dagger}	✓	✓	○
Scheil's rule based on expt'l. TTT	✗	✗	○
Cooling rate at Ae_1	✗	✓	Not Applicable

†) ✓: Good agreement

○: Acceptable agreement

✗: No agreement

Chapter 7

SUMMARY AND RECOMMENDATION

7.1 Summary of The Study

A critical examination of Scheil's additivity rule for predicting the incubation time (transformation start time) of the austenite to pearlite transformation was carried out in this study.

The concept of an "ideal" *TTT* curve was introduced to account for the fractional incubation time consumed during cooling to the test temperature. The ideal *TTT* curve is considered to depend only on the steel's chemistry and its austenite grain size prior to the transformation.

The ideal *TTT* curve was derived either from the data of the controlled isothermal or the controlled cooling experiments. In the controlled isothermal experiments, known initial cooling rates were used to cool the specimen to the desired isothermal temperature. The measured times to the start of transformation were used to deduce the ideal incubation time at that temperature.

Alternatively, cooling experiments with controlled cooling rates were performed to generate a controlled cooling transformation diagram, which was then used to back calculate the "ideal" *TTT* curve by applying the inverse of Scheil's additivity rule.

In this study, the "ideal" *TTT* curve for the transformation to pearlite in a eutectoid steel was found to have the following form:

$$\tau(T) = 32.5 \frac{\exp\left(\frac{125.6 \text{ kJ/mol}}{RT}\right)}{(\Delta T)^{4.15}}$$

Although this expression for the incubation time is semi-empirical in nature, Kirkaldy^[76] used a similar form for describing the 0.1% onset of transformation assuming that site saturation occurs early in the reaction, and the incubation process is governed by slow growth. The characteristic feature of the derived "ideal" *TTT* curve was quite similar to that published in ASM Atlas of Isothermal Diagrams. The temperature at which the shortest incubation time occurs (i.e., the "nose" temperature) was found to be about 520 °C, while the published literature suggested it to be around 530 °C. However, the minimum transformation time (the "nose" time) of the "ideal" *TTT* curve is shorter than that of traditional *TTT* curve.

When the "ideal" *TTT* curve was used to predict the start of the transformation to pearlite by applying Scheil's additivity rule, good agreement between the measured and the predicted results was found for the continuous cooling and the Stelmor simulation situations.

Reasonable agreement was also found when the technique was applied to the non-continuous cooling situations, although the predictions were consistently early by 10 seconds. However, when the results are compared to those obtained by other reported methods for predicting the start of transformation, the predictions based on the "ideal" *TTT* curve were found to give better agreement for a wider range of thermal history conditions.

7.2 Recommendation for Further Development

This study has been conducted within a specified time frame, therefore, the primary objective of the project has been focused on establishing a method for predicting the onset of the austenite to pearlite decomposition during continuous and non-continuous cooling conditions.

While the objective of this study has been met by the development of an "ideal" *TTT* curve, further investigation is still necessary to develop a detailed understanding of the concept, and to generalise it to a wider range of steel chemistries so that it can be applied to current steel processing.

To develop a detailed theoretical understanding of the additivity concept, further investigation in the following areas have been considered necessary:

- i)* The early nucleation site saturation constitutes one prerequisite condition for a reaction to be additive, which consequently, enables the isothermal transformation data to be used to describe the transformation behaviour during cooling. Tests are needed to establish whether site saturation occurred under cooling conditions employed in this study, and if this site saturation condition changed in any of the controlled cooling experiments.

- ii)* The equation used to describe the incubation time function (i.e. equation 2.18) was a simple equation which assumes the effects of composition to be constant. It is adequate for describing the *C* curve of plain carbon steels. However, to account for the interaction of alloying elements, a more vigorous approach such as that which has been pursued by Bhadeshia^[58] would be needed. This would be essential when the model is used to assess the effect of alloying elements on the transformation behaviour and the final microstructure of a steel in response to a particular industrial cooling schedule.

REFERENCES

- 1 McLean, D.W.: *Wire & Wire Products*, **39**, 1964, pp. 1606-1609
- 2 Adcock, J.N.: *J. Iron Steel Inst.*, **200**, 1962, pp. 909-913
- 3 Yada, H.; Mori, T.; Murakami, M.; Tominaga, J. & Ochiai, M.: *Nippon Steel Tech. Report*, **21**, 1983, pp. 203-215
- 4 Speich, G.R.; Cuddy, L.J.; Gordon, C.R. & DeArdo, A.J.:
"Phase Transformation in Ferrous Alloys", Proc. Int. Conf., Philadelphia-1983
 Ed. by: Marder, A.R. & Goldstein, J.I., AIME, Warrendale, PA-1984, pp 341-389
- 5 DeArdo, A.J.: *Can. Metall. Quart.*, **27**, 1988, pp. 141-154
- 6 Machida, M. *et.al.*: *Tetsu-to-Hagane*, **68**, 1982, pp. A223-226
- 7 Southwick, P.D.:
"Accelerated Cooling of Steel", Proc. Int. Symp., Pittsburg-1985
 AIME, Warrendale, PA-1986
- 8 Ruddle, G.E. & Crawley, A.F.:
Proc. "Int. Symp. Accelerated Cooling of Steel", Winnipeg-1987
 Pergamom, Oxford-1988
- 9 Wu, C.T. & Pan, Y. T.:
"Processing, Microstructure and Prperties of HSLA Steels",
 Proc. Int. Symp., Pittsburg-1987
 Ed. by: DeArdo, A.J., TMS, Warrendale, PA-1988, pp 345-358
- 10 Abe, T.; Tsukada, K. & Kozasu, I.: *Tetsu-to-Hagane*, **74**, 1988, pp. 505-512
- 11 Korchynsky, M.:
"Accelerated Cooling of Steel", Proc. Int. Symp., Pittsburg-1985
 Ed. by Southwick, P.D., AIME, Warrendale, PA-1986, pp. 3-14
- 12 Amin, R.K.. & Pickering, F.B.:
"Thermomechanical Processing of Microalloyed Austenite",
 Proc. Int. Conf., Pittsburg-1981, Ed. by: DeArdo, A.J.; Ratz, G.A. & Wray, P.J.,
 AIME, Warrendale, PA-1982, pp. 377-403
- 13 Ouchi, C.; Sampei, T. & Kozasu, I.: *Trans. ISIJ*, **22**, 1982, pp. 214-222

- 14 Hulka, K. *et.al.*:
"Processing, Microstructure and Properties of HSLA Steels",
 Proc. Int. Symp., Pittsburg-1987
 Ed. by: DeArdo, A.J., TMS, Warrendale, PA-1988, pp. 117-132
- 15 Vlad, C.M.:
"Accelerated Cooling of Steel", Proc. Int. Symp., Pittsburg-1985
 Ed. by: Southwick, P.D., AIME, Warrendale, PA-1986, pp. 435-446
- 16 Tamura, I.; Ouchi, C.; Tanaka, T. & Sekine, H.:
"Thermomechanical Processing of High Strength Low Alloy Steels",
 Butterworths, London-1988, Chapter 8, p. 140 & Chapter 12, p.226
- 17 Matsumura, Y. & Yada, H.: *Trans. ISIJ*, **27**, 1987, pp. 492
- 18 Beynon, J.H.; Gloss, R. & Hodgson, P.D.: *Materials Forum*, **16**, 1992, pp. 37-42
- 19 Irvine, K.J.; Gladman, T.; Orr, J. & Pickering, F.B.: *J. Iron & Steel Inst.*, **208**, 1970, pp. 717-726
- 20 Swinden, D.J. & Woodhead, J.H: *J. Iron & Steel Inst.*, **209**, 1971, pp. 883-899
- 21 Tanaka, T.: *Int. Metals Rev.*, **26**, 1981, pp. 185-212
- 22 Abe, T.; Tsukada, K. & Kozasu, I.: *Tetsu-to-Hagane*, **74**, 1988, pp. 505-512
- 23 Tamura, I.: *Trans. ISIJ.*, **27**, 1987, pp. 763-779
- 24 Campbell, P.C.; Hawbolt, E.B. & Brimacombe, J.K: *Metall. Trans. A*, **22A**, 1991, pp. 2779-2790
- 25 Simon, P.; Economopoulos, M. & Nilles, P.: *Iron & Steel Engineer*, March-1984, pp. 55-57
- 26 Killmore, C.; Barrett, J.F. & Williams, J.G.:
"Accelerated Cooling of Steel", Proc. Int. Symp., Pittsburg-1985
 Ed. by Southwick, P.D., AIME, Warrendale, PA-1986, pp. 541-558
- 27 Oouchi, C. *et.al.*: *Tetsu-to-Hagane*, **67**, 1981, pp. 969-978
- 28 Davenport, E.S. & Bain, E.C.: *Trans. AIME*, **90**, 1930, pp. 117-144

- 29 "Atlas of Isothermal and Continuous Cooling Transformation Diagrams",
American Society for Metals, Metals Park, OH-1977
- 30 Atkins, M.:
"Atlas of Continuous Cooling Transformation Diagrams for Engineering Steels",
American Society for Metals, Metals Park, OH, 1980
- 31 Cias, W.W.:
"Phase Transformation Kinetics & Hardenability of Medium-C Alloy Steels",
Climax Molybdenum, Greenwich, Connecticut-1973
- 32 Weiss, I & Jonas, J.J.: *Metall. Trans. A*, **10A**, 1979, pp. 831-840
- 33 Akben, M.G.; Weiss, I & Jonas, J.J.: *ACTA Metall.*, **29**, 1981, pp. 111-121
- 34 Yamamoto, S.; Ouchi, C. & Osuka, T.:
"Thermomechanical Processing of Microalloyed Austenite",
Proc. Int. Conf., Pittsburg-1981, Ed. by: DeArdo, A.J.; Ratz, G.A. & Wray, P.J.,
AIME, Warrendale, PA-1982, pp. 613-639
- 35 Wang, G.L. & Akben, M.G.:
"HSLA Steels",
Ed. by: DeArdo, TMS, Warrendale, PA-1988, pp. 79-90
- 36 Bain, E.C.: *Trans. Amer. Soc. Steel Treating*, **20**, 1932, pp. 385
- 37 Davenport, E.S.: *Trans. ASM*, **27**, 1939, pp. 837
- 38 Scheil, E.: *Arch. Eisenhüttenwesen*, **8**, 1935, pp. 565-567 (Translation)
- 39 Shteinberg, S.S.: *Metallurg*, **13**, 1938, pp. 7-12 (Translation)
- 40 Manning, G.K. & Lorig, C.H.: *Trans. AIME*, **167**, 1946, pp. 442-466
- 41 Jaffe, L.D.: *Trans. AIME*, **176**, 1948, pp. 363-383
- 42 Moore, P.T.: *J. Iron & Steel Inst.*, **177**, 1954, pp. 305-311
- 43 Pumphrey, W.I. & Jones, F.W.: *J. Iron Steel Inst.*, **159**, 1948, pp. 137-144
- 44 Grange, R.A. & Kiefer, J.M.: *Trans. ASM*, **29**, 1941, pp. 85-116
- 45 Cahn, J.W.: *ACTA Metall.*, **4**, 1956, pp. 572-575

- 46 Christian, J.W.:
"The Theory of Transformations in Metals and Alloys",
 Part I, 2nd Ed., Pergamon Press, Oxford-1975, pp. 542-548
- 47 Avrami, M.: *J. Chem. Phys.*, **7**, 1939, pp. 1103-1012
J. Chem. Phys., **8**, 1940, pp. 212-224
J. Chem. Phys., **9**, 1941, pp. 177-184
- 48 Cahn, J.W.: *ACTA Metall.*, **4**, 1956, pp. 449-459
- 49 Cahn, J.W.: *Trans. AIME*, **209**, 1957, pp. 140-144
- 50 Lange, W.F.; Enomoto, M. & Aaronson, H.I.: *Metall. Trans. A*, **19A**, 1988, pp. 427-440
- 51 Kuban, M.B.; Jayaraman, R.; Hawbolt, E.B. & Brimacombe, J.K.: *Metall. Trans. A*, **17A**, 1986, pp. 1493-1503
- 52 Kamat, R.G.; Hawbolt, E.B.; Brown, L.C. & Brimacombe, J.K.: *Metall. Trans. A*, **23A**, 1992, pp. 2469-2480
- 53 Russell, K.C.: *Acta Metall.*, **17**, 1969, pp. 1123-1131
- 54 Russell, K.C.: *Adv. Colloid & Interface Science*, **13**, 1980, pp. 205-318
- 55 Lange, W.F.; Enomoto, M. & Aaronson: *Int. Mat. Rev.*, **34**, 1989, pp. 125-150
- 56 Kaufman, L.; Radcliffe, S.V. & Cohen, M.:
"Decomposition of Austenite by Diffusional Processes",
 AIME Symp., Philadelphia - 1960
 Ed. by Zackay, V.F. & Aaronson, H.I., Interscience, New York - 1962, pp 313-351
- 57 Porter, D.A. & Easterling, K.E.:
Phase Transformations in Metals & Alloys,
 Van Nostrand, London - 1989, pp 66-68
- 58 Bhadeshia, H.K.H.: *Met. Sci.*, 1982, **16**, pp 159-165
- 59 Shiflet, G.J.; Bradley, J.R. & Aaronson, H.I.: *Metall. Trans. A*, **9A**, (7), 1978, pp.999-1008
- 60 McLellan, R.B. & Dunn, W.W.: *Scrip. Metall.*, **4**, 1970, pp.321-326

- 61 Zener, C.: *Trans. AIME*, **167**, 1946, pp. 550-595
- 62 Fisher, J.C.:
"Thermodynamics in Physical Metallurgy",
 ASM, Cleveland-1950, pp. 201-241
- 63 Turnbull, D.: *ACTA Metall.*, **3**, 1955, pp. 55-63
- 64 Hillert, M.: *Jernkont. Ann.*, **141**, 1957, pp. 757-789
- 65 Hawbolt, E.B.; Chau, B. & Brimacombe, J.K.: *Metall. Trans. A*, **14A**, 1983, pp. 1803-1815
- 66 Hawbolt, E.B.; Chau, B. & Brimacombe, J.K.: *Metall. Trans. A*, **16A**, 1985, pp. 565-578
- 67 Umemoto, M.; Horiuchi, K. & Tamura, I.: *Trans. ISIJ*, **22**, 1982, pp. 854-861
- 68 Umemoto, M.; Horiuchi, K. & Tamura, I.: *Trans. ISIJ*, **23**, 1983, pp. 690-695
- 69 Umemoto, M.; Nishioka, N. & Tamura, I.:
"Heat Treatment Shanghai '83", Int. Congress on Heat Treatment, Shanghai-1983
 Ed. by T. Bell, Metals Society, London - 1984, p. 5.35
- 70 Fernandes, F.M.B.; Denis, S. & Simon, A: *Mat. Sci. & Tech.*, **1**, 1985, pp. 838-844
- 71 Denis, S.; Gautier E.; Simon, A & Beck, G.: *Mat. Sci. & Tech.*, **1**, 1985, pp. 805-814
- 72 Umemoto, M.; Komatsubara, N. & Tamura, I.:
"Proc. Int. Conf. Solid-Solid Phase Transformations",
 Ed. by Aaronson, H.I. et. al., TMS-AIME, Pittsburg, 1981, pp. 1111-1115.
- 73 Buza, G.; Hougardy, H.P. & Gergely, M.: *Steel Research*, **57**, 1986, pp. 650-653
- 74 Buza, G.; Hougardy, H.P. & Gergely, M.: *Steel Research*, **61**, 1990, pp. 478-481
- 75 Reti, T.; Gergely, M. & Tardy, P.: *Mat. Sci. & Tech.*, **3**, 1987, pp. 365-371
- 76 Kirkaldy, J.S.; Thomson, B.A. & Baganis, E.A.:
"Hardenability Concept with Applications to Steels",
 Ed. by: Doan, D.V. & Kirkaldy, J.S., AIME, Warrendale, PA-1978, pp. 82-125
- 77 Pham, T.T.: *BHP-MRL Tech. Note*, September 1989

- 78 Kirkaldy, J.S. & Baganis, E.A.: *Metall. Trans. A*, **9A**, 1978, pp. 495-501
- 79 Kirkaldy, J.S. & Venugopalan, D.:
"Phase Transformations in Ferrous Alloys",
Ed. by: Marder, A.R. & Goldstein, J.I., AIME, Warrendale, PA-1983, pp. 125-148
- 80 Kirkaldy, J.S. & Shama, R.C.: *Script. Metall.*, **16**, 1982, pp. 1193-1198
- 81 Shimizu, N. & Tamura, I.: *Trans. ISIJ*, **17**, 1977, pp. 469-476
- 82 Wierszylowski, I.A.: *Metall. Trans. A*, **22A**, 1991, pp. 993-999
- 83 Eldis, G.T.:
"Hardenability Concept with Applications to Steels",
Ed. by: Doan, D.V. & Kirkaldy, J.S., AIME, Warrendale, PA-1978, pp. 126-148
- 84 Andrews, K.W.: *J. Iron and Steel Inst.*, **203**, 1965, pp. 721-727
- 85 Hurkmans, A. *et. al.*:
"Accelerated Cooling of Steel", Proc. Int. Symp., Pittsburg-1985
Ed. by Southwick, P.D., AIME, Warrendale, PA-1986, pp. 481-499
- 86 Hogg, R.V. & Ledolter, J.:
"Applied Statistics for Engineers and Physical Scientists",
Macmillan Pub., New York-1992, Chapter 5, p. 187
- 87 Holman, J.P.:
"Heat Transfer", 7th ed.,
McGraw-Hill, New York-1990, Table A-2, p. 653
- 88 White, F.M.:
"Heat and Mass Transfer",
Addison-Wesley, Ontario-1988, p. 194-196
- 89 Vander Voort, G.F.:
"Metallography Principles and Practice",
McGraw-Hill, New York-1984, p. 436
- 90 Sellars, C.M.:
"Hot Working and Forming Processes",
Ed. by: Sellars, C.M. & Davies, D.J., Metals Society, London-1980, pp. 3-15

REFERENCES

- 91 Cuddy, L.J.: *Metall. Trans. A*, **12A**, 1981, pp. 1313-1320
- 92 Cuddy, L.J.: *Metall. Trans. A*, **15A**, 1984, pp. 87-98

APPENDICES

A.1 Thermal Analysis of the Tubular Specimen

The dilatometer specimens were tubular with an outer diameter of $8mm$, an inner diameter of $6mm$ and $20mm$ long. Temperature changes during testing were obtained by a controlled flow of He gas down the center of the tubular specimens. Thus, during cooling, the sample losses heat via radiation from the outer surface and convection to the gas from the inside surface, the temperature being monitored by an intrinsic thermocouple spot welded on the outer surface at mid length position.

The follow analysis estimates the magnitude of the thermal gradient that may exist through the wall thickness of the dilatometer specimen during cooling.

A.1.1 The Biot Modulus

To determine the severity of the thermal gradient within the tubular wall of the dilatometer specimen, it is necessary to examine the Biot number (or modulus) of the specimen. The Biot number, Bi , which is a measure of conduction resistance relative to convection resistance, is defined as:

$$Bi = L \frac{h}{k} \quad \dots(A.1 - 1)$$

where L , h and k are the characteristic length, the heat transfer coefficient and the thermal conductivity, respectively.

It is assumed that the radiation losses from the outer surface are negligible compared to the heat lost by convection from the inner surface; this assumption corresponds to the most severe thermal gradient through the wall, where the outer surface is essentially adiabatic.

The thermal characteristic length of the specimen, L , can be evaluated as follows:

$$L = \frac{V}{A} \quad \dots(A.1-2)$$

where V and A are volume and surface area of the specimen exposed to cooling, respectively.

$$\begin{aligned} L &= \frac{\pi(r_o^2 - r_i^2)}{2\pi r_i} \\ &= \frac{(r_o^2 - r_i^2)}{2r_i} \end{aligned} \quad \dots(A.1-3)$$

where r_i and r_o are the inner and outer radius, respectively. Using (A.1-3) in (A.1-1), the Biot number for the hollow cylindrical specimen is:

$$Bi = \frac{(r_o^2 - r_i^2)}{2r_i} \left(\frac{h}{k} \right) \quad \dots(A.1-4)$$

Data for the thermal conductivity, k , of eutectoid steel in the temperature range of experimentation, was obtained from Holman,^[87] and is approximately $30 \text{ W/m}^\circ\text{C}$. The corresponding value for Bi of the dilatometer specimen is, where $r_i=3\text{mm}$ and $r_o=4\text{mm}$:

$$\begin{aligned} Bi &= \frac{(4^2 - 3^2) \cdot 10^{-6}}{2 \times 3 \cdot 10^{-3}} \left(\frac{h}{30} \right) \\ &= 3.89 \cdot 10^{-5} \times h \end{aligned} \quad \dots(\text{A.1-5})$$

Given that the internal thermal gradient will become significant when the value of $Bi \geq 0.1$ ^[88], this defines an upper limit for h , according to equation (A.1-5), of $2570 \text{ W/m}^2^\circ\text{C}$.

A.1.2 Estimation of the Effective Heat Transfer Coefficient

After being austenitised at 900°C for 2 minutes, the specimen was rapidly cooled to 780°C and allowed to equilibrate for 1 minute before being cooled rapidly to the isothermal holding temperature. Although heat is extracted by the flow of He gas through the inside of the specimen, the temperature is obtained from a thermocouple located on the outer surface.

To determine the approximate heat transfer coefficient at the internal surface, as a first approximation, it is assumed that the temperature recorded on the outer surface closely represents that on the inner surface. This allows the use of a lump solution of the form:

$$\ln \frac{(T_{iso} - T_g)}{(780 - T_g)} = -\frac{\bar{h}A}{\rho c_p V} t \quad \dots(A.1 - 6)$$

where T_{iso} is the isothermal holding temperature, T_g is the He gas temperature and \bar{h} is the effective heat transfer coefficient over the temperature range under consideration. Taking the density and the specific heat of steel^[87] to be 7800 kg/m^3 and $473 \text{ kJ/kg}^\circ\text{C}$, respectively, and together with the result of (A.1-3), equation (A.1-6) becomes:

$$\ln \frac{(T_{iso} - T_g)}{(780 - T_g)} = -2.32 \cdot 10^{-4} \times \bar{h} t \quad \dots(A.1 - 7)$$

The effective heat transfer coefficient, which characterises the heat extraction process, can then be determined based on the thermal data recorded.

Figure A.1-1 shows the early part of the thermal history of a test in which the specimen was rapidly cooled from 780 to 650 °C, where it was then held isothermally. It took approximately 1 second to reach the temperature of 650 °C, from 780 °C, which corresponds to a mean cooling rate of about 140 °C/s. Taking the gas temperature to be 20 °C, equation (A.1-7) yields an effective heat transfer coefficient of $807 \text{ W/m}^2^\circ\text{C}$, which is less than one third of the critical value of $2570 \text{ W/m}^2^\circ\text{C}$, as estimated in part A.1.1. This also means that the approximation used in deriving the effective heat transfer coefficient was in fact plausible.

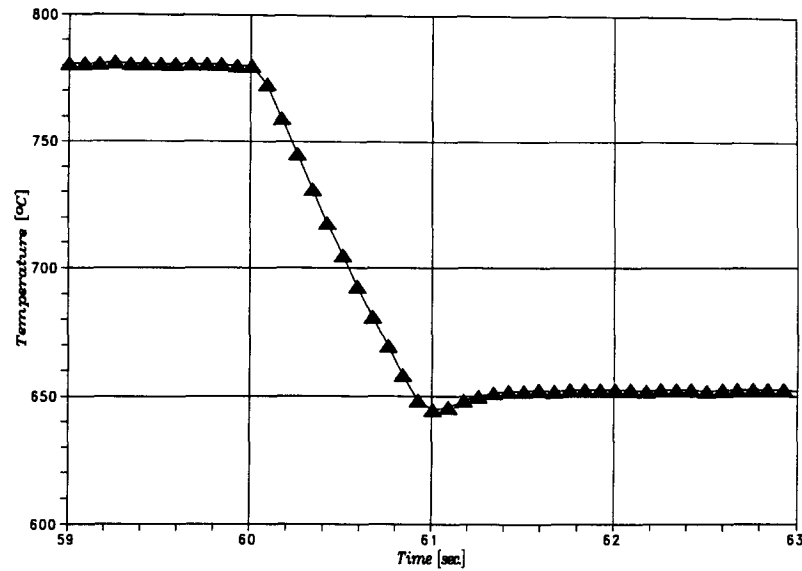


Figure A.1-1: Thermal history of a specimen that was rapidly cooled to 650 °C where it is held isothermally.

A.1.3 Conclusion

Thermal analysis of the tubular steel specimen, which was internally cooled by the flow of He gas to affect changes in temperature, indicates that the temperature gradient through the 1mm wall is insignificant. The Biot number for the cooling process is estimated to be 0.032, indicating a reasonably uniform through thickness temperature during cooling. Thus, the temperature reading on the outer surface may be interpreted as the mean temperature of the specimen.

A.2 Thermal Gradients inside the Tubular Specimen

Thermal analysis by means of the Biot modulus provides a qualitative estimation of the thermal gradient across the wall thickness of the tubular specimen. However, variation in temperatures in the annular cross section can also occur circumferential, which could severely affect the dilatometry results.

In this study, the diametral dilations of the specimen were monitored by using a LVDT C-strain device, which measures the average changes in dimension of the specimen in the cross sectional plane. Meanwhile, the temperature changes were monitored by a means of a thermocouple which spot welded on the outer surface of the specimen, located approximately on this plane. Thus, in the ideal case, the temperature field is expected to be uniform in this cross sectional plane.

However, the contact of this instrument onto the specimen disturbs the uniformity of the temperature field, and hence, steps were taken to minimise the disturbance. The severity of the contact effect was assessed by metallography. Transformation to pearlite was allowed to take place upto 20% inside a specimen, then rapidly cooled to room temperature where the microstructure in the cross sectional plane was examined. From this assessment, it was found that the tips of sample-supporting rods must be reduced to yield a uniform microstructure in the cross sectional plane.

A.3 Determination of the Transformation Start

Figure A.3-1 shows the temperature and dilation history of a specimen which was control cooled at a constant rate of $3\text{ }^{\circ}\text{C/s}$, after being isothermally held at $780\text{ }^{\circ}\text{C}$ for 1 minute to remove any thermal gradient through the wall.

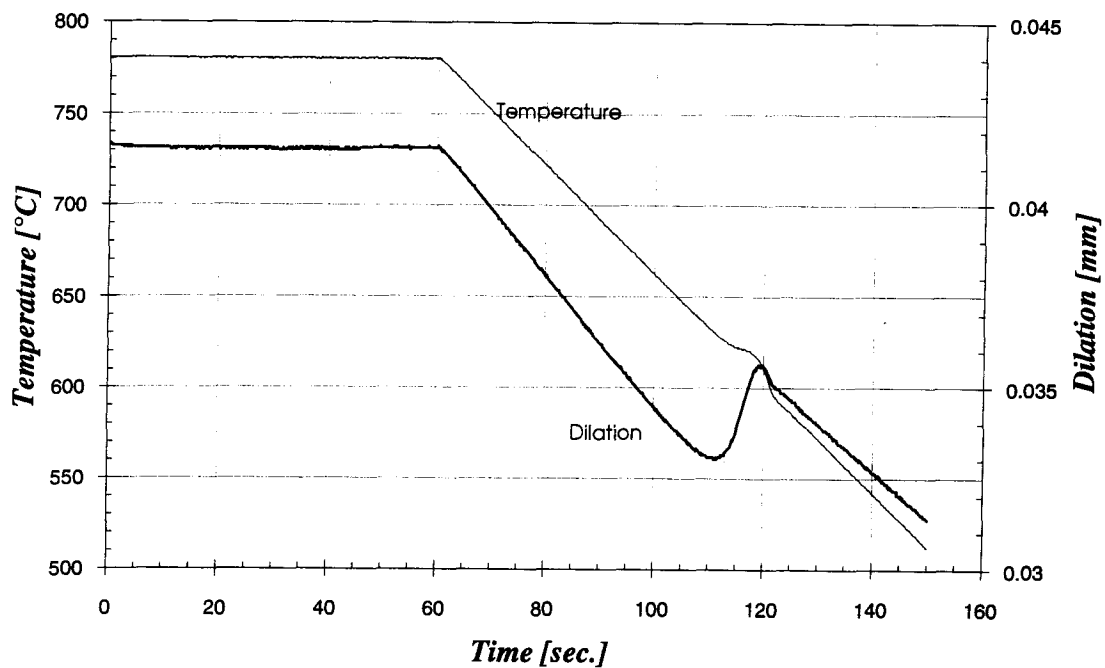


Figure A.3-1: Thermal and dilation history of a specimen undergoing controlled cooling at $3\text{ }^{\circ}\text{C/s}$, after being isothermally held at $780\text{ }^{\circ}\text{C}$ for 1 minute.

The change in dimension of the specimen during cooling is assumed to consist of two major components: the contraction due to change in sample temperature, and the expansion due to volume increase associated with the transformation from austenite to pearlite taken place

within the sample. The contraction of the austenite phase due to decreasing temperature down to 730 °C was assumed to vary linearly with temperature. A linear regression was carried out and the line of best fit is shown in Figure A.3-2, together with the measured data.

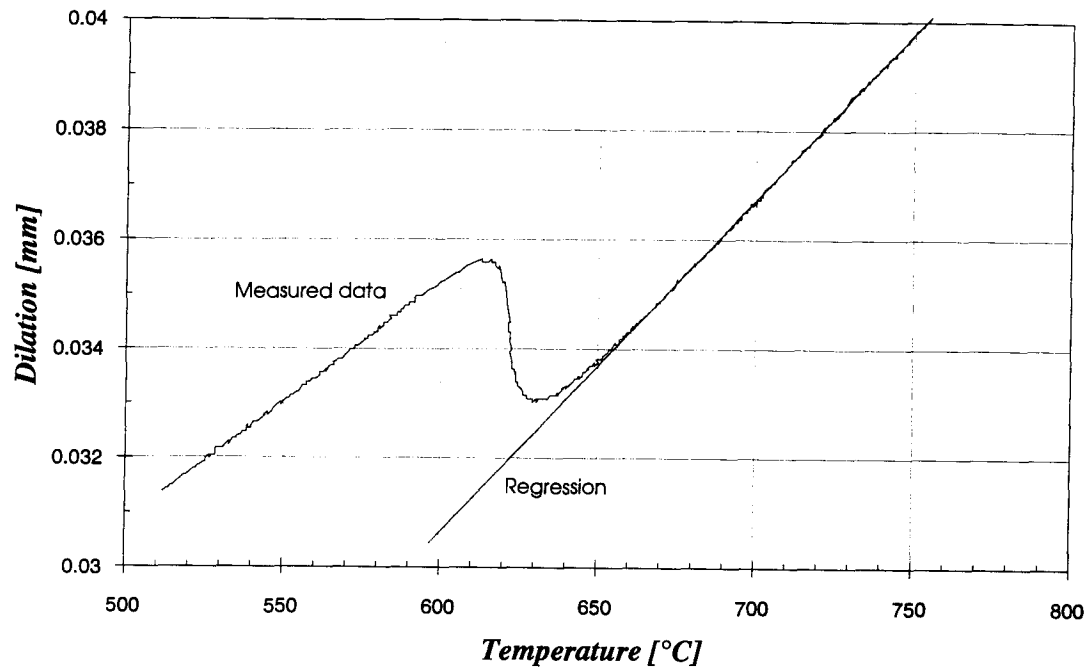


Figure A.3-2: Relationship between the dilation and temperature throughout the experiment, with a linear correlation exists in the pre-transformed region.

It can be seen from the result that the linearity assumption is, in fact, reasonable; excellent fit is observed in the region above 670 °C. However, at lower temperatures, due to the formation of pearlite, the measured data deviated from this linear relationship, as can be depicted in Figure A.3-2.

To maintain consistency throughout the analysis, a statistical data analysis method^[86] was employed. In the region where the dilation varies linearly with temperature, the scatter of the measured data about the regression was assumed to have a normal distribution with a standard deviation σ . A plot of the scatter in the 3 °C/s controlled cooling test is shown in Figure A.3-3, where deviation was defined as scatter of the data about the regressed mean dilation.

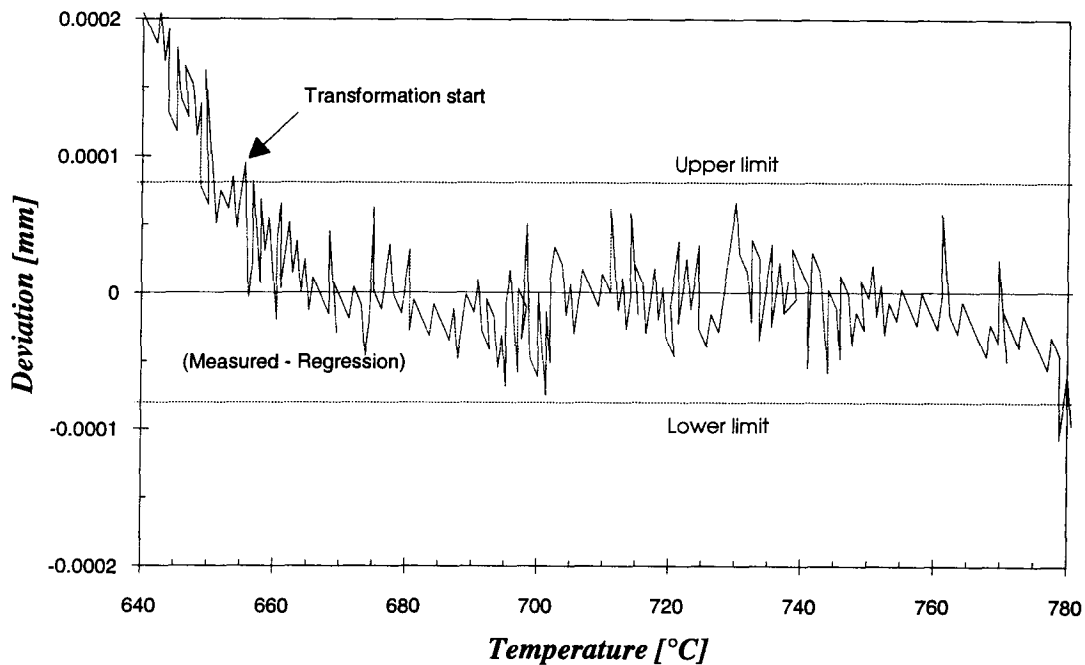


Figure A.3-3: Deviation of the measured data from the linear regression, delineating the start of transformation to pearlite.

The linear relationship was no longer obeyed when the transformation to pearlite began; in this region the deviation is amplified beyond the control limit, which has been defined as 3σ .^[86] This point was taken to be the start of transformation to pearlite, as indicated in Figure A.3-3.